

Article

Comprehensive Metabolic Profiling of Euphorbiasteroid in Rats by Integrating UPLC-Q/TOF-MS and NMR as Well as Microbial Biotransformation

Sijia Xiao ^{1,†}, Xike Xu ^{1,†}, Xintong Wei ^{2,†}, Jiayun Xin ^{1,2}, Shanshan Li ³, Yanhui Lv ^{1,2}, Wei Chen ¹, Wenlin Yuan ¹ , Bin Xie ¹, Xianpeng Zu ^{1,*}  and Yunheng Shen ^{1,*} 

¹ School of Pharmacy, Naval Medical University, Shanghai 200433, China

² School of Pharmacy, Shandong University of Traditional Chinese Medicine, Jinan 250355, China

³ School of Pharmaceutical Sciences and Yunnan Key Laboratory of Pharmacology for Natural Products, Kunming Medical University, Kunming 650500, China

* Correspondence: zuxianpeng@163.com (X.Z.); shenyunheng@hotmail.com (Y.S.)

† These authors contributed equally to this work.

Abstract: Euphorbiasteroid, a lathyrane-type diterpene from *Euphorbiae semen* (the seeds of *Euphorbia lathyris* L.), has been shown to have a variety of pharmacological effects such as anti-tumor and anti-obesity. This study aims to investigate the metabolic profiles of euphorbiasteroid in rats and rat liver microsomes (RLMs) and *Cunninghamella elegans* bio-110930 by integrating ultra-performance liquid chromatography-quadrupole time-of-flight-mass spectrometry (UPLC-Q/TOF-MS), UNIFI software, and NMR techniques. A total of 31 metabolites were identified in rats. Twelve metabolites (M1–M5, M8, M12–M13, M16, M24–M25, and M29) were matched to the metabolites obtained by RLMs incubation and the microbial transformation of *C. elegans* bio-110930 and their structures were exactly determined through analysis of NMR spectroscopic data. In addition, the metabolic pathways of euphorbiasteroid were then clarified, mainly including hydroxylation, hydrolysis, oxygenation, sulfonation, and glycosylation. Finally, three metabolites, M3 (20-hydroxyl euphorbiasteroid), M24 (epoxylathyrol) and M25 (15-deacetyl euphorbiasteroid), showed significant cytotoxicity against four human cell lines with IC₅₀ values from 3.60 μM to 40.74 μM. This is the first systematic investigation into the in vivo metabolic pathways of euphorbiasteroid and the cytotoxicity of its metabolites, which will be beneficial for better predicting the metabolism profile of euphorbiasteroid in humans and understanding its possible toxic material basis.

Keywords: euphorbiasteroid; metabolic pathway in vivo; UPLC-Q/TOF-MS; *Cunninghamella elegans*; microbial biotransformation



Citation: Xiao, S.; Xu, X.; Wei, X.; Xin, J.; Li, S.; Lv, Y.; Chen, W.; Yuan, W.; Xie, B.; Zu, X.; et al. Comprehensive Metabolic Profiling of Euphorbiasteroid in Rats by Integrating UPLC-Q/TOF-MS and NMR as Well as Microbial Biotransformation. *Metabolites* **2022**, *12*, 830. <https://doi.org/10.3390/metabo12090830>

Academic Editor: Ala F. Nassar

Received: 9 August 2022

Accepted: 30 August 2022

Published: 2 September 2022

Publisher's Note: MDPI stays neutral with regard to jurisdictional claims in published maps and institutional affiliations.



Copyright: © 2022 by the authors. Licensee MDPI, Basel, Switzerland. This article is an open access article distributed under the terms and conditions of the Creative Commons Attribution (CC BY) license (<https://creativecommons.org/licenses/by/4.0/>).

1. Introduction

Euphorbiae semen, known as “Qian-Jin-Zi” in China, is the dried and ripe seeds of *Euphorbia lathyris* L. According to the 2020 edition of the Chinese Pharmacopoeia, *Euphorbiae semen* could be clinically used either alone or in combination with other herbal medicines as remedies for reducing water and phlegm retention, promoting blood circulation, removing blood stasis, curing tinea and scabies, and treating amenorrhea, snakebites, terminal schistosomiasis, anuria, and constipation. It is worth noting that *Euphorbiae semen* was listed as one of the 28 toxic Chinese herbal medicines in the Chinese Pharmacopoeia [1]. It has been proven to exhibit a strong stimulating effect on the gastrointestinal tract, and its intensity is three times that of croton oil. The main toxic components of *Euphorbiae semen* are diterpenoids, identified by means of fractionation. Euphorbiasteroid (M0, Figure 1), a natural lathyrane-type diterpenoid, was deemed as one of the intestinal tract stimulant constituents to induce diarrhea [2]. Moreover, euphorbiasteroid has the potential to reverse resistance to anticancer drugs in MES-SA/Dx5 cells [3], and also exhibits anti-obesity [4],

and anti-tumor activities [5], meaning that it has broad biomedical research prospects. Previous studies have shown that euphorbiasteroid is one of the main toxic and active components of *Euphorbiae semen*, and has also been used as a quantitative index for quality control in Chinese pharmacopoeia [6]. However, there is still a lack of research on the metabolism of diterpenoids in euphorbiasteroid, which brings difficulties to the clinically safe use of this toxic Chinese medicine. Thus, in order to further understand the toxic and active mechanisms of euphorbiasteroid, a systematic study of its metabolic profiles is of great significance.

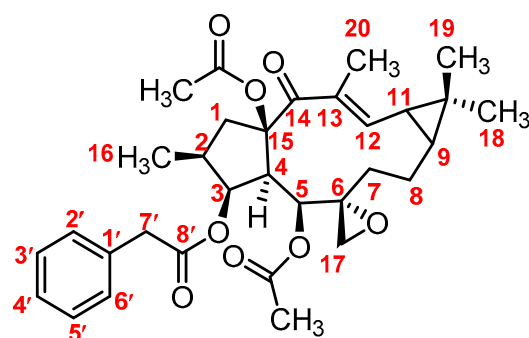


Figure 1. The chemical structure of euphorbiasteroid (M0).

The in-depth study of drug metabolism can clarify the metabolic pathways as well as the toxic and active mechanisms of drugs so as to ensure their safety and lay a theoretical foundation for clinical application and toxic and side effect detection [7]. Therefore, it is of great significance and value to establish a sensitive and reliable analytical method for the identification of drug metabolites. Liquid chromatography (LC) is one of the main methods used to analyze active pharmaceutical ingredients (APIs) in American and European Pharmacopoeia, and has been combined with a variety of detectors, such as fluorescence detectors, electrochemical detectors or flame photometric detectors. However, these detectors cannot clearly identify compounds separated by LC. In contrast, high performance liquid chromatography-mass spectrometry (HPLC-MS), with liquid chromatography as the separation system and mass spectrometry as the detection system, combines the high separation capability of HPLC for complex samples with the high selectivity and sensitivity of mass spectrometry and its ability to provide relative molecular mass and structural information, perfectly compensating for this deficiency [8,9]. Especially, ultra-performance liquid chromatography-quadrupole time-of-flight-mass spectrometry (UPLC-Q/TOF-MS) combined with the computer-aided identification platform Waters UNIFI, has become a powerful analytical tool, which has the advantages of accurate mass measurement, efficient separation technology, and rapid identification of metabolites, and has been widely applied in the metabolism research of traditional Chinese medicine in recent years [10]. However, the main disadvantage of mass spectrometry analysis is that the molecular weight of structural characterization depends on the collision-induced dissociation of protonated molecular ions of target compounds, so it cannot provide accurate metabolite structure in most cases [11]. Nuclear magnetic resonance (NMR) is a complementary analytical method, which can characterize metabolites in more detail. The advantages of the combination of UPLC-Q/TOF-MS and NMR have been verified in several reports in recent years [12–14]. However, the sensitivity of NMR is not as good as that of mass spectrometry, and the presence of impurities in the sample has great influence on NMR signal. Therefore, it is necessary to separate the analyte from the impurity well and obtain enough quantity for structural identification by NMR. Generally, supplementary methods can be used to obtain a sufficient sample amount of metabolites, including chemical methods [11] and small experimental animal models [15], microsomal preparations [16,17], enzyme-catalyzed reactions [18,19], microbial transformation [11,20] and so on. Compared with other methods, microbial transformation is more convenient and economical, especially with the

advantages of in vitro large-scale preparation [20–24]. In particular, the filamentous zygote fungus *C. elegans* has been shown to possess a human-like cytochrome P450 monooxygenase system, including the CYP509A1 isoenzyme that is similar to the CYP51 family, thus producing similar metabolic profiles to mammalian animals [25,26]. Sufficient samples for structural characterization based on NMR techniques as well as the evaluation of bioactivity and toxicity can thus be acquired. Therefore, a combination of in vivo animal experiments and in vitro microbial transformation will contribute to accurately elucidating the structures of metabolites.

The current work aimed to identify the metabolites of euphorbiasteroid in rats and in vitro models (RLMs and *C. elegans* bio-110930), by using UPLC-Q/TOF-MS and the UNIFI platform as well as NMR technique, and to rationalize the elimination mechanism of euphorbiasteroid, in which the biotransformation based on the fungus *C. elegans* bio-110930 and chemical hydrolysis were applied to prepare the samples of potential metabolites. This method has been used in the previous research of our research group and is reasonable [27]. Finally, a total of 31 metabolites in vivo, including four phase II metabolites, were detected and identified. Additionally, the structures of 12 metabolites were accurately characterized and confirmed by structural elucidation based on NMR technique and by comparing the chromatography retention times and mass spectra with those of standard compounds from the biotransformation products of *C. elegans* bio-110930. Then, the metabolic pathway of euphorbiasteroid in rats was rationally elucidated on the basis of the study of metabolism in vivo and in vitro. The cytotoxic assay showed that three metabolites of euphorbiasteroid (M3, M24–M25) have cytotoxicity on four strains of human cells (SH-SY5Y, LO2, AC-16, and HK-2) with the IC₅₀ values from 3.60 μM to 40.74 μM, while euphorbiasteroid did not show cytotoxicity on the same cell lines (IC₅₀ > 50 μM). Therefore, our research findings will provide new insights into the metabolism mechanism of euphorbiasteroid and the possible toxicity of the metabolites, be beneficial for understanding the in vivo elimination process of euphorbiasteroid, and provide data support and reference for safe, reasonable and controllable clinical application of *Euphorbia* semen.

2. Materials and Methods

2.1. Chemicals and Reagents

Euphorbiasteroid was purchased from Chengdu Herbpurify Co., Ltd. (Chengdu, China). Soybean oil was bought from Ron Pharm (Shanghai) Co., Limited. Sabouraud dextrose broth was procured from Qingdao Hope Bio-Technology Co., Ltd. (cat no. HB0233, Qingdao, China). Sabouraud dextrose agar was obtained from Solarbio (cat no. P9240, Beijing, China). The fungal strain, *Cunninghamella elegans* (bio-110930), was purchased from the Beijing baioubowei Biotechnology Co., Ltd. (Beijing, China). Pooled rat liver microsomes (RLM), Gentest™ NADPH regenerating system solution A (26.1 mM β-nicotinamide adenine dinucleotide phosphate (NADP⁺), 66 mM D-glucose-6-phosphate (Glc-6-P), 66 mM magnesium chloride (MgCl₂) in water and solution B (40 U/mL Glc-6-P dehydrogenase (Glc-6-P-DH) in sodium citrate (0.05 mM)), and 0.1 M PBS buffer were purchased from IPHASE Biosciences (Beijing, China). Column chromatography (CC) was performed using Sephadex LH-20 gel (GE Medical Systems Ltd., Buckinghamshire, UK). Ethyl acetate and acetone were analytical grade from Shenyang Chemical Reagent Co., Ltd. (Shenyang, China). LC-MS-grade acetonitrile, methanol and formic acid were purchased from Fisher-Scientific (Fair Lawn, NJ, USA) and were used in the mobile phase and sample preparation. LC-MS-grade leucine enkephalin was obtained from Sigma-Aldrich (St. Louis, MO, USA). Ultra-pure water was purified by a Milli-Q system (Millipore, Bedford, MA, USA). All other reagents were of analytical reagent grade. SH-SY5Y neuroblastoma cells, LO2 cells, AC-16 cells, and HK-2 cells were purchased from Shanghai Institute of Biochemistry and Cell Biology, Chinese Academy of Sciences (Shanghai, China). CCK-8 assay kit was obtained from Beyotime Biotechnology (Shanghai, China). 6 cm/10 cm Petri dishes and 96-well plates were obtained from Corning Incorporated (Corning, NY, USA).

2.2. Instrumentation and Analysis Conditions

For metabolite separation and detection, chromatographic analyses were performed using a Waters Acquity UPLC I-class system (Waters, Milford, MA, USA), equipped with an auto-sampler, a binary solvent delivery system, an online degasser, and a photodiode array detector. An ACQUITY UPLC[®] HSS T3 column (2.1 × 150 mm, 1.8 μm, Waters) protected with a HSS T3 VanGuard[™] Pre-Column 3/Pk (2.1 × 5.0 mm, 1.8 μm, Waters) was used. The optimized parameters were set as follows: the mobile phase consisted of eluent A (0.1% formic acid in water, *v/v*) and eluent B (acetonitrile). The flow rate was 0.3 mL/min. The column and auto-sampler temperatures were maintained at 40 °C and 4 °C, respectively. The gradient elution program was optimized as follows: 0–9 min, 30–70% B; 9–13 min, 70–90% B; 13–17 min, 90–100% B; 17–20 min, 100–100% B.

The mass spectrometry detection was performed on the SYNAPT G2-Si HDMS system, equipped with an electrospray ionization (ESI) source (Waters Corp., Manchester, UK). A positive ion mode was conducted in this analysis. Mass spectrometry conditions were finally set as follows: capillary voltage of 3.0 kV, cone voltage of 40 V, source temperature of 120 °C, and de-solvation temperature of 400 °C. Nitrogen was used as the desolvation and cone gas with a flow rate of 800 and 50 L/h, respectively, and the full-scan mass range was set as *m/z* 50–1500 Da. In the auto mass spectrometry mode, the collision-induced dissociation energies were set at 0 eV for the precursor ion at the low-energy mode, and the collision-induced dissociation energies were set from 2 to 10 eV for the high-energy mode. Real-time data were calibrated using an external reference (LockSpray[™]) at a concentration of 0.2 ng/mL with an infusion flow rate of 5 μL/min, generating a reference ion for the positive ion mode (*m/z* 556.2771) during the UPLC-MS analysis. Data were acquired and processed using MassLynx[™] NT 4.1 software (Waters, Milford, MA, USA).

Accurate molecular weights of some metabolites were acquired using an Agilent 6520 Accurate Mass quadrupole time-of-flight mass spectrometer (Q-TOF MS; Agilent Technologies, Santa Clara, CA, USA). The capillary voltage of the ion source was set at 3.0 kV in positive ion mode. Nitrogen was used as the de-solvation and nebulizing gas at a constant temperature of 350 °C. The scan range was set at *m/z* 100–1500 Da.

The isolation and purification of metabolites were achieved using an Agilent 1200 series Semi-preparative High Performance Liquid Chromatography (HPLC) system (Palo Alto, CA, USA) consisting of a G1311A quat pump solvent delivery system, a G1379A degasser unit, a G1313A autosampler, and a G1315B DAD detector. The preparation was performed with a Zorbax SB-C18 (5 μm, 9.4 mm × 25 cm) column (Agilent Technologies, Santa Clara, CA, USA). The wavelength was set at 280 nm.

Nuclear magnetic resonance (NMR) spectra of euphorbiasteroid and metabolites were measured on Bruker AV-500 spectrometers (Faellanden, Switzerland) using tetramethylsilane as an internal standard.

2.3. Animal and Drug Administration

Male Sprague-Dawley rats (200–220 g) were commercially supplied by Shanghai Sippr-BK Laboratory Animal Co., Ltd. (Shanghai, China) and were housed in a humidity- and temperature-controlled room (50 ± 10% and 22–24 °C) with a 12-h light/dark cycle. The experimental rats were allowed to access food and water *ad libitum* and acclimatized to the conditions mentioned above for a week, then fasted overnight but with free access to water before the experiments. Euphorbiasteroid was dissolved in soybean oil solution (containing 0.5% ethanol) to form a concentration of 10 mg/mL. A single dose of 100 mg/kg euphorbiasteroid was orally administered to rats and the same concentration of soybean oil solution (containing 0.5% ethanol) was administered as a blank control. All animal procedures were performed in accordance with the Guidelines for Care and Use of Laboratory Animals of Naval Medical University and approved by the Animal Ethics Committee of Naval Medical University.

2.4. Sample Collection of Blood, Urine, and Feces

Blood samples (0.5 mL) were collected from six rats through the orbital sinus before administration (blank sample) and 0.25, 0.5, 1, 2, 4, 6, and 12 h after administration. Plasma samples were prepared by centrifugation at 4000 rpm for 10 min. For urine and feces sampling, 12 rats were divided into an administration group and a blank group, and were placed separately in stainless steel metabolic cages. Urine and feces samples were collected in containers surrounded by ice over 0–6, 6–12, and 12–24 h after drug administration. The mixed urine samples were centrifuged at 4000 rpm for 10 min at 4 °C to obtain the supernatants, and fecal samples were left in a cool and dry place until dry. All the biological samples were frozen at –80 °C before analysis.

2.5. Preparation of Blood, Urine, and Feces Samples

An aliquot of 200 µL of plasma and urine samples was put in a 1.5 mL tube, respectively. 800 µL of acetonitrile was added and vortexed for 5 min to extract metabolites. Feces samples (1.0 g) were crushed and then ultrasonically extracted with acetonitrile (10 mL) for 30 min. All the above-mentioned mixtures were centrifuged at 13,000 rpm at 4 °C for 10 min. The supernatants were then transferred and evaporated to dryness under a nitrogen stream at 30 °C. The residues were dissolved in 100 µL of methanol and then centrifuged at 13,000 rpm at 4 °C for 10 min. All supernatants were injected into the UPLC-Q/TOF-MS system for analysis.

2.6. In Vitro Incubation of Euphorbiasteroid with Rat Liver Microsomes

The microsomal incubation approach was based on previous metabolism studies published by Wintermeyer et al. [28] and Franziska et al. [17]. A 200 µL incubation system containing 10 µL of solution A, 2 µL of solution B, 5 µL of rat liver microsomes (20 mg/mL) and 182 µL 0.1 M PBS buffer (pH = 7.4) was constructed. The above solution was heated in a 37 °C water bath, then 1 µL of euphorbiasteroid (dissolved in DMSO solution, 10 mM) was used to start the reaction, and the mixture was then incubated at 37 °C for 1 h. The reactions were terminated by the addition of 200 µL of ice-cold acetonitrile. The mixture was then centrifuged at 13,000 rpm for 10 min, and a 2-µL aliquot of the supernatant was directly injected into the UPLC-Q-TOF-MS system.

2.7. Microbial Transformation of Euphorbiasteroid

The biotransformation process was conducted at two scales: preliminary screening and preparative. Preliminary screening scale biotransformation of euphorbiasteroid was carried out in 250 mL Erlenmeyer flasks containing 100 mL of liquid medium. The flasks were placed on a rotary shaker (160 rpm, 28 °C). A standard two-stage fermentation protocol was employed in all experiments [29,30]. After 2 days of pre-culture, the substrates of 5 mg (dissolved in 0.5 mL of acetone) were added into each flask. Taking 1 mL samples on days 0, 2, 4, 7, 10, and 14, samples were centrifuged and the degree of transformation was compared to controls on TLC and HPLC, and a 2-µL aliquot of the supernatant was directly injected into the UPLC-Q-TOF-MS system. Culture controls consisted of sterile medium, in which microorganisms were grown under identical conditions without substrate. Substrate controls were composed of sterile medium and the same amount of substrate incubated under the same conditions without microorganisms.

2.8. Preparation of the Transformation Products of Euphorbiasteroid

The preparative scale biotransformation of euphorbiasteroid was carried out in 50 1000 mL Erlenmeyer flasks, each containing 400 mL of sterilized potato medium. The flasks were placed on a rotary shaker operating at 160 rpm at 28 °C. After 48 h of pre-culture, 20 mg of substrates in 2 mL of acetone were added to each flask. After 12 days of incubation, the culture was pooled and filtered. The filtrate was extracted three times with an equal volume of EtOAc and concentrated under reduced pressure to dryness.

The crude extract (3.58 g) was partitioned by MPLC column chromatography (CC) eluted with gradient MeOH/H₂O (100% H₂O, 25 mL/min, 3 h; 30% MeOH, 25 mL/min, 3 h; 50–70% MeOH, 25 mL/min, 3 h; 70–100% MeOH, 25 mL/min, 3 h) into 6 fractions (Fr. A–Fr. F). On the basis of TLC and HPLC analysis as well as comparing the LC-MS/MS data with those of the metabolites in rats, the metabolites of euphorbiasteroid were detected in Fr. B–Fr. E. Then, Fr. B (285.9 mg) was separated by Sephadex LH-20 CC (3 × 150 cm) with MeOH/H₂O (30%) as eluent to give the fractions Fr. B1–Fr. B4. Next, Fr. B2 (64.5 mg) was purified by semi-preparative HPLC on a Zorbax SB-C18 semi-preparative column with the mobile phase consisting of methanol and 0.1% formic acid water (42:58, *v/v*) to obtain compound **9** (4.7 mg, *t_R* = 24.5 min). Fr. C (56.2 mg) was applied to Sephadex LH-20 CC (3 × 150 cm) eluting with MeOH/H₂O (50%) to yield Fr. C1–Fr. C3. Then, Fr. C2 (10.2 mg) was further separated using semi-preparative HPLC (50% MeOH in water, *v/v*, 2.0 mL/min) to give compound **6** (2.9 mg, *t_R* = 51.5 min). Fr. D (78.9 mg) was purified by Sephadex LH-20 CC (3 × 150 cm) eluting with MeOH/H₂O (50%) to afford four fractions (Fr. D1–Fr. D4). Then, Fr. D2 (40.4 mg) was further separated using semi-preparative HPLC (35% CH₃CN in water, *v/v*, 2.0 mL/min) to give compounds **2** (1.7 mg, *t_R* = 58.6 min) and **5** (3.6 mg, *t_R* = 62.3 min). Fr. E (345.0 mg) was subjected to Sephadex LH-20 CC (3 × 150 cm) eluting with MeOH/H₂O (50%) to provide five fractions (Fr. E1–Fr. E5). Then, Fr. E2 (30.3 mg) was submitted to semi-preparative HPLC eluting with MeOH–H₂O (60:40, *v/v*, 2.0 mL/min) to yield compound **12** (10.6 mg, *t_R* = 31.5 min). Fr. E3 (38.5 mg) was purified by semi-preparative HPLC eluting with MeOH–H₂O (65:35, *v/v*, 2.0 mL/min) to obtain compounds **1** (7.1 mg, *t_R* = 19.2 min), **4** (2.5 mg, *t_R* = 30.5 min), and **3** (2.0 mg, *t_R* = 37.0 min). Compounds **7** (1.7 mg, *t_R* = 26.5 min) and **8** (4.3 mg, *t_R* = 38.5 min) were acquired by semi-preparative HPLC (MeOH/H₂O, 65%, 2 mL/min) from Fr. E4 (19.2 mg).

Compounds **10** and **11** were obtained by the hydrolysis of euphorbiasteroid. 210 mg of euphorbiasteroid was dissolved in 45 mL of MeOH, and 3 mL of 1.54 mol/L KHCO₃ aqueous solution was added dropwise to this solvent with stirring. The mixture was stirred and hydrolyzed at 30 °C. After 5 days, methanol was removed by evaporation under vacuum, and the remaining solution was then extracted three times with 200 mL of solution (ethyl acetate: water = 1:1). The combined organic layer was evaporated under a vacuum. The ethyl acetate extract (184.5 mg) was re-dissolved in 10 mL of methanol, followed by Sephadex LH-20 CC (3 × 150 cm) eluting with MeOH/H₂O (50%) to afford four fractions (Fr. 1–Fr. 5). Fr. 2 was further purified using semi-preparative HPLC (50% MeOH in water, *v/v*, 2.0 mL/min) to afford compounds **10** (44.6 mg, *t_R* = 5.5 min) and **11** (45.7 mg, *t_R* = 19.5 min).

2.9. Cell Culture and Cell Cytotoxicity Assay

Cell cytotoxicity was determined by the CCK-8 assay. Four strains of human cells (SH-SY5Y) were seeded in 96-well plates at a density of 3 × 10³ cells/well under 37 °C and 5% CO₂ for 12 h and subsequently treated with the test sample solution (euphorbiasteroid and its metabolites, 10 µL) for 72 h. After treatment, each well with 10 µL CCK-8 reagent was incubated for 1–2 h in the incubator. Afterwards, the optical OD-value was measured at 450 nm through a microplate reader. Three multiple wells were set as parallel experimental groups.

3. Results and Discussion

3.1. Mass Fragmentation Behavior Analyses of Euphorbiasteroid

In order to obtain the overall fragmentation profile of euphorbiasteroid, the standard solution of euphorbiasteroid was analyzed by UPLC-Q/TOF-MS, which is helpful to better understand the MS/MS spectrum of its metabolites. The parent drug euphorbiasteroid had a protonated molecular ion [M + H]⁺ at *m/z* 553.2809 with a retention time of 12.67 min. In the MS/MS spectrum, it had the characteristic and most abundant fragment ion at *m/z* 297.1850, derived from the loss of two CH₃COOH and one C₆H₅CH₂COOH neutral molecules, which was further fragmented to form ion peaks at *m/z* 279.1746, *m/z*

269.1898, and m/z 251.1794 via loss of H_2O , CO , and $CO + H_2O$, respectively. Moreover, the fragment ions at m/z 493.2587 and m/z 417.2276 were produced by losing CH_3COOH and $C_6H_5CH_2COOH$ from the ion at m/z 553.2794, respectively, which further yielded the fragment ions at m/z 433.2371 ($[M + H - 2CH_3COOH]^+$) and m/z 357.2062 ($[M + H - CH_3COOH - C_6H_5CH_2COOH]^+$). In addition, the fragment ion at m/z 315.1953 resulted from the ions at m/z 433.2371 and m/z 357.2062 by loss of $C_6H_4CH_2CO$ and CH_2CO , respectively, which further lost a water to form ion at m/z 297.1850. Therefore, CH_3COOH (m/z 493.2587), $C_6H_5CH_2COOH$ (m/z 417.2276), $CH_3COOH + C_6H_5CH_2COOH$ (m/z 433.2371) and $2 CH_3COOH + C_6H_5CH_2COOH$ (m/z 279.1746) were the characteristic product ions of euphorbiasteroid. Mass spectra and the fragmentation scheme for euphorbiasteroid were shown in Figure 2. The 1H NMR and ^{13}C NMR spectral data of euphorbiasteroid are listed in Tables 1–3, with the carbon position labeled as shown in Figure 1.

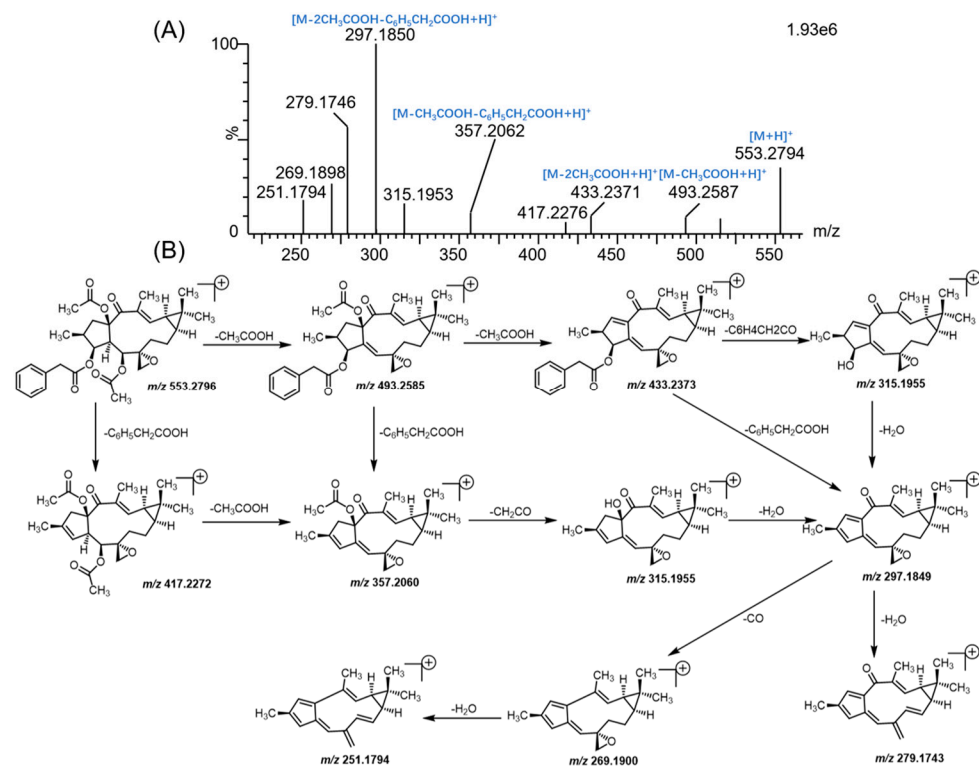


Figure 2. The mass spectrum (A) and proposed MS/MS fragmentation patterns (B) of euphorbiasteroid.

3.2. Identification of Metabolites of Euphorbiasteroid In Vitro and In Vivo

First, the metabolites of euphorbiasteroid in rats (plasma, urine, and feces), RLMs, and *C. elegans* culture medium were predicted by setting the prototype components and potential biological metabolic reactions in UNIFI 4.1 software. Then, the predicted metabolites in each sample were further compared according to the characteristic mass spectrum behaviors (including parent ions, internal cleavage in the ion source, and characteristic fragment ions of each metabolite) and retention times. A total of 31 metabolites identified in vitro and in vivo are listed in Table 4. The retention times, precursor molecular ions, and key fragments of euphorbiasteroid and its metabolites are listed in Table 4. The extracted ion chromatograms and product ion spectra of metabolites are shown in Figures 3 and 4.

Table 1. The ¹H NMR data for euphorbiasteroid and its transformation products (1–6).

Position	M0 ^a	1 ^a	2 ^a	3 ^a	4 ^a	5 ^a	6 ^b
1a	3.32 (dd, 8.15, 13.68)	3.29 (dd, 8.29, 14.22)	3.32 (dd, 8.38, 14.26)	3.30 (dd, 8.67, 14.43)	3.19 (dd, 8.25, 14.37)	3.35 (dd, 8.25, 14.28)	3.20 (dd, 8.16, 12.94)
1b	1.35 (dd, 12.01, 13.68)	1.34 (dd, 12.42, 14.22)	1.37 (dd, 12.22, 14.26)	1.36 (dd, 12.80, 14.43)	1.04 (dd, 12.60, 14.37)	1.42 (dd, 12.26, 14.28)	1.41 (t, 12.94)
2	2.08 (m)	2.06 (overlap)	2.07 (m)	2.07 (m)	2.01 (m)	2.10 (overlap)	2.05 (overlap)
3	5.48 (brt., 3.32)	5.47 (brt., 3.15)	5.47 (brt., 3.05)	5.50 (s)	5.49 (brt., 2.84)	5.50 (brt, 3.03)	5.37 (brt, 2.95)
4	1.86 (dd, 3.32, 9.28)	1.85 (dd, 3.20, 9.35)	1.86 (dd, 3.05, 9.30)	1.92 (d, 9.66)	1.84 (dd, 2.84, 9.11)	1.88 (dd, 3.03, 9.17)	1.83 (dd, 2.95, 9.02)
5	6.24 (d, 9.28)	6.23 (d, 9.23)	6.23 (d, 9.30)	6.25 (d, 9.66)	6.28 (d, 9.11)	6.25 (d, 9.17)	6.29 (d, 9.02)
7a	1.87 (m)	2.14 (m)	2.12 (m)	2.14 (m)	2.12 (overlap)	2.10 (overlap)	2.10 (m)
7b	0.92 (m)	0.94 (t, 13.16)	0.93 (m)	0.98 (m)	0.94 (m)	0.93 (m)	0.97 (t, 13.93)
8a	2.10 (m)	2.06 (overlap)	2.07 (m)	2.12 (overlap)	2.09 (m)	2.07 (m)	2.00 (m)
8b	1.72 (m)	1.77 (m)	1.72 (m)	1.75 (m)	1.72 (m)	1.68 (m)	1.80 (m)
9	1.09 (m)	1.21 (m)	1.09 (ddd, 3.78, 8.08, 12.07)	1.21 (overlap)	1.09 (m)	1.09 (m)	1.33 (m)
11	1.48 (dd, 8.11, 11.34)	1.65 (dd, 8.39, 11.13)	1.48 (dd, 8.08, 11.35)	1.71 (m)	1.48 (dd, 8.20, 11.42)	1.47 (dd, 8.10, 11.39)	1.78 (overlap)
12	6.59 (d, 11.34)	6.59 (d, 11.23)	6.59 (dd, 1.05, 11.35)	6.71 (d, 12.41)	6.59 (dd, 1.05, 11.30)	6.59 (d, 11.39)	6.69 (d, 11.28)
16	0.66 (d, 6.63)	0.65 (d, 6.65)	0.67 (d, 6.66)	0.67 (d, 6.63)	0.33 (d, 6.70)	0.69 (d, 6.69)	0.76 (d, 6.72)
17a	2.48 (d, 3.37)	2.49 (d, 3.35)	2.49 (d, 3.40)	2.62 (s)	2.50 (d, 3.24)	2.50 (d, 3.24)	2.56 (d, 3.54)
17b	2.30 (brt., 3.37)	2.29 (brt., 3.35)	2.31 (brt., 3.40)	2.50 (s)	2.28 (brt., 3.24)	2.21 (brt., 3.24)	2.20 (t, 3.54)
18a	1.20 (s)	3.52 (d, 11.25)	1.20 (s)	1.21 (s)	1.21 (s)	1.20 (s)	3.48 (d, 11.25)
18b		3.44 (d, 11.25)					3.38 (d, 11.25)
19	1.21 (s)	1.27 (s)	1.21 (s)	1.22 (s)	1.22 (s)	1.21 (s)	1.27 (s)
20a	1.84 (s)	1.84 (s)	1.84 (brd, 0.81)	4.42 (d, 12.38)	1.83 (d, 1.04)	1.84 (s)	1.79 (d, 0.93)
20b				4.28 (d, 12.38)			
				3-O-phenylacetyl			
2'	7.25 (overlap)	7.25 (overlap)	7.13 (d, 7.92)	7.27 (overlap)	7.37 (m)		
3'	7.30 (m)	7.29 (td, 1.21, 7.19)	6.76 (d, 7.92)	7.31 (t, 7.26)	7.32 (overlap)	6.90 (overlap)	6.86 (dd, 0.96, 7.35)
4'	7.27 (t, 7.76)	7.24 (m)		7.26 (overlap)	7.30 (overlap)	7.18 (t, 7.45)	7.08 (t, 7.35)
5'	7.30 (m)	7.29 (td, 1.21, 7.19)	6.76 (d, 7.92)	7.31 (t, 7.26)	7.32 (overlap)	6.88 (overlap)	6.78 (t, 7.35)
6'	7.25 (overlap)	7.25 (overlap)	7.13 (d, 7.92)	7.27 (overlap)	7.37 (m)	7.11 (dd, 1.45, 7.45)	7.18 (d, 7.35)
7'a	3.58 (2H, d, 3.21)	3.56 (2H, 2.71)	3.50 (2H, d, 3.57)	3.58 (2H, s)	5.10 (2H, s)	3.70 (d, 15.10)	3.65 (d, 15.64)
7'b						3.55 (d, 15.10)	3.55 (d, 15.64)
8'							
				5-OAc			
C=O							
CH ₃	2.02 (s)	2.00 (s)	2.01 (s)	2.03 (s)	2.12 (s)	1.94 (s)	2.06 (s)
				15-OAc			
C=O							
CH ₃	2.12 (s)	2.12 (s)	2.13 (s)	2.12 (s)	2.19 (s)	2.17 (s)	2.08 (s)

^a Measured at 500 MHz in CDCl₃. ^b Measured at 500 MHz in CD₃OD.

Table 2. The ¹H NMR data for euphorbiasteroid and its transformation products (7–12).

Position	M0 ^a	7 ^a	8 ^a	9 ^a	10 ^a	11 ^a	12 ^a
1a	3.32 (dd, 8.15, 13.68)	3.40 (dd, 8.21, 14.17)	3.39 (dd, 8.03, 13.95)	3.30 (dd, 8.24, 14.25)	3.00 (dd, 9.58, 13.84)	3.15 (dd, 9.37, 14.18)	3.21 (dd, 7.65, 13.47)
1b	1.35 (dd, 12.01, 13.68)	1.52 (dd, 12.25, 14.17)	1.50 (dd, 12.69, 13.95)	1.36 (dd, 12.35, 14.25)	2.26 (dd, 6.08, 13.84)	0.91 (dd, 11.72, 14.18)	1.16 (overlap)
2	2.08 (m)	2.16 (m)	2.16 (m)	2.08 (m)	2.04 (m)	2.04 (m)	1.96 (m)
3	5.48 (brt., 3.32)	5.51 (brt., 3.08)	5.53 (brs.)	5.49 (brt., 2.80)	4.25 (brs)	5.46 (s)	5.37 (s)
4	1.86 (dd, 3.32, 9.28)	1.89 (dd, 3.08, 9.06)	1.89 (m)	1.87 (overlap)	1.28 (brs)	1.76 (dd, 2.84, 9.91)	1.79 (overlap)
5	6.24 (d, 9.28)	6.22 (d, 9.06)	6.24 (d, 8.82)	6.22 (d, 9.10)	4.39 (brs)	5.92 (d, 9.91)	6.21 (d, 8.90)
7a	1.87 (m)	2.08 (m)	2.08 (m)	2.17 (m)	2.04 (m)	2.12 (dd, 6.42, 13.12)	2.08 (overlap)
7b	0.92 (m)	0.92 (t, 13.69)	0.93 (t, 12.07)	1.01 (t, 13.36)	1.05 (m)	0.87 (m)	0.90 (m)
8a	2.10 (m)	2.04 (m)	2.05 (m)	2.11 (m)	1.77 (m)	2.08 (overlap)	2.08 (overlap)
8b	1.72 (m)	1.73 (m)	1.71 (m)	1.77 (m)	1.67 (dd, 10.35, 13.80)	1.69 (m)	1.69 (m)
9	1.09 (m)	1.08 (m)	1.08 (m)	1.90 (overlap)	1.16 (m)	1.09 (m)	1.07 (brt., 8.28)
11	1.48 (dd, 8.11, 11.34)	1.48 (dd, 8.07, 11.30)	1.48 (dd, 8.37, 11.17)	2.44 (dd, 9.04, 11.20)	1.42 (dd, 8.48, 11.02)	1.48 (dd, 8.21, 11.60)	1.46 (dd, 8.28, 11.11)
12	6.59 (d, 11.34)	6.60 (d, 11.03)	6.60 (d, 11.17)	6.47 (d, 11.20)	6.68 (d, 8.48)	7.32 (overlap)	6.56 (d, 11.11)
16	0.66 (d, 6.63)	0.87 (d, 6.72)	0.85 (d, 6.39)	0.67 (d, 6.58)	1.11 (d, 6.84)	0.81 (d, 6.69)	0.42 (d, 6.46)
17a	2.48 (d, 3.37)	2.48 (d, 3.46)	2.49 (d, 3.33)	2.53 (d, 3.11)	2.64 (d, 3.79)	2.41 (d, 2.24)	2.46 (s)
17b	2.30 (brt., 3.37)	2.32 (brt, 3.46)	2.32 (brs)	2.29 (brt., 3.11)	2.59 (d, 3.79)	2.27 (s)	2.26 (s)
18	1.20 (s)	1.19 (s)	1.19 (s)		1.14 (s)	1.21 (s)	1.19 (s)
19	1.21 (s)	1.19 (s)	1.19 (s)	1.44 (s)	1.15 (s)	1.25 (s)	1.20 (s)
20	1.84 (s)	1.85 (s)	1.85 (s)	1.88 (s)	1.89 (s)	1.78 (s)	1.81 (s)
3-O-phenylacetyl							
2'	7.25 (overlap)	5.54 (brs)	5.66 (s)	7.27 (overlap)		7.32 (overlap)	
3'	7.30 (m)	7.54 (d, 10.30)	3.72 (brs)	7.31 (td, 0.83, 7.12)		7.36 (t, 7.35)	7.01 (d, 7.36)
4'	7.27 (t, 7.76)	6.07 (dt, 1.81, 10.30)	4.25 (brd., 5.56)	7.26 (m)		7.28 (t, 7.21)	7.20 (t, 7.36)
5'	7.30 (m)	4.26 (d, 7.49)	6.07 (m)	7.31 (td, 0.83, 7.12)		7.36 (t, 7.35)	6.92 (t, 7.36)
6'	7.25 (overlap)	3.76 (m)	6.15 (d, 10.14)	7.27 (overlap)		7.32 (overlap)	7.12 (d, 7.36)
7'a	3.58 (2H, d, 3.21)	2.67 (m)	3.69 (m)	3.58 (2H, s)		3.67 (d, 16.65)	3.81 (d, 13.39)
7'b		2.54 (m)	2.55 (m)	7.27 (overlap)		3.64 (d, 16.65)	3.35 (d, 13.39)
8'							
5-OAc							
C=O							
CH ₃	2.02 (s)	2.00 (s)	2.00 (s)	2.02 (s)		2.08 (s)	2.04 (s)

Table 2. Cont.

Position	M0 ^a	7 ^a	8 ^a	9 ^a	10 ^a	11 ^a	12 ^a
C=O				15-OAc			
CH ₃	2.12 (s)	2.13 (s)	2.13 (s)	2.13 (s)			2.17 (s)
				Glc			
1''							4.81 (d, 6.77)
2''							3.69 (overlap)
3''							3.49 (m)
4''							3.69 (overlap)
5''							3.65 (m)
6''a							3.89 (d, 13.27)
6''b							3.85 (d, 13.27)

^a Measured at 500 MHz in CDCl₃.

Table 3. The ¹³C NMR data for euphorbiasteroid and its transformation products (1–12).

Position	M0 ^a	1 ^a	2 ^a	3 ^a	4 ^a	5 ^a	6 ^b	7 ^a	8 ^a	9 ^a	10 ^a	11 ^a	12 ^a
1	47.9(d)	47.8 (t)	47.9 (t)	47.3 (t)	47.5 (t)	47.7(t)	48.3 (t)	47.9 (t)	47.9 (t)	47.9 (t)	48.2 (t)	49.9 (t)	47.7 (t)
2	37.7 (s)	37.7 (d)	37.8 (d)	37.8 (d)	37.8 (d)	37.8 (d)	38.5 (d)	37.8 (d)	37.9 (d)	37.7 (d)	37.6 (d)	37.2 (d)	37.6 (d)
3	80.6(d)	80.6 (d)	80.6 (d)	80.6 (d)	82.6 (d)	81.5 (d)	80.9 (d)	79.8 (d)	79.8 (d)	80.6 (d)	78.9 (d)	82.8 (d)	81.0 (d)
4	49.9 (s)	49.9 (d)	49.9 (d)	49.9 (d)	49.7 (d)	49.7 (d)	50.6 (d)	49.9 (d)	49.7 (d)	50.0 (d)	53.4 (d)	51.6 (d)	49.7 (d)
5	65.2(d)	65.1 (d)	65.2 (d)	65.1 (d)	65.1 (d)	65.3 (d)	65.9 (d)	65.2 (d)	65.2 (d)	65.0 (d)	66.5 (d)	66.0 (d)	65.2 (d)
6	58.9 (s)	58.9 (s)	59.0 (s)	58.6 (s)	58.9 (s)	58.9 (s)	59.4 (s)	59.0 (s)	59.0 (s)	58.7 (s)	60.8 (s)	58.9 (s)	58.9 (s)
7	33.5(d)	33.4 (t)	33.5 (t)	33.4 (t)	33.4 (t)	33.5 (t)	34.1 (t)	33.5 (t)	33.4 (t)	32.9 (t)	32.1 (t)	33.9 (t)	33.4 (t)
8	20.0(d)	19.7 (t)	20.1 (t)	20.0 (t)	20.1 (t)	20.1 (t)	20.6 (t)	20.0 (t)	20.0 (t)	19.3 (t)	19.7 (t)	20.0 (t)	20.0 (t)
9	34.8 (s)	30.2 (d)	34.8 (d)	35.8 (d)	34.8 (d)	34.8 (d)	31.1 (d)	34.8 (d)	34.8 (d)	32.9 (d)	34.7 (d)	35.7 (d)	34.8 (d)
10	25.6 (s)	31.0 (s)	25.7 (s)	26.9 (s)	25.7 (s)	25.7 (s)	32.1 (s)	25.6 (s)	25.6 (s)	29.9 (s)	25.1 (s)	26.4 (s)	25.6 (s)
11	29.0 (d)	25.2 (d)	29.0 (d)	29.0 (d)	29.1 (d)	29.0 (d)	26.2 (d)	29.1 (d)	29.1 (d)	30.1 (d)	28.7 (d)	29.3 (d)	29.0 (d)
12	143.7 (t)	142.1 (d)	143.8(d)	147.6(d)	143.8(d)	143.7(d)	144.1(d)	143.7(d)	143.7(d)	137.9(d)	144.6(d)	150.8(d)	143.7(d)
13	136.0(d)	136.7 (s)	136.0 (s)	138.4 (s)	136.0 (s)	136.0 (s)	136.7 (s)	136.0 (s)	135.9 (s)	139.0 (s)	136.2 (s)	135.1 (s)	135.9 (s)
14	196.9(d)	196.9 (s)	196.9(s)	198.4 (s)	196.6(s)	196.7(s)	197.3 (s)	196.9 (s)	196.8 (s)	197.2 (s)	202.8 (s)	199.3 (s)	197.3 (s)
15	91.7 (s)	91.7 (s)	91.8 (s)	91.5 (s)	91.5 (s)	91.6 (s)	92.2 (s)	91.8 (s)	91.7 (s)	91.7 (s)	88.4 (s)	88.7 (s)	91.6 (s)
16	13.5(q)	13.5 (q)	13.6 (q)	13.5 (q)	12.8 (q)	13.4 (q)	13.8 (q)	14.0 (q)	14.0 (q)	13.5 (q)	13.9 (q)	14.2 (q)	13.1 (q)
17	55.4 (t)	55.3 (t)	55.4 (t)	56.2 (t)	55.3 (t)	55.2 (t)	53.4 (t)	55.4 (t)	55.3 (t)				
18	28.9(q)	71.2 (t)	28.9 (q)	28.8 (q)	28.9 (q)	28.9 (q)	70.9 (t)	16.7 (q)	16.7 (q)	179.8 (s)	28.7 (q)	29.0 (q)	28.9 (q)
19	16.8(q)	12.5 (q)	16.8 (q)	16.7 (q)	16.8 (q)	16.8 (q)	12.9 (q)	28.9 (q)	28.9 (q)	10.4 (q)	15.8 (q)	16.3 (q)	16.7 (q)
20	12.3 (t)	12.4 (q)	12.4 (q)	58.1 (t)	12.3 (q)	12.4 (q)	12.5 (q)	12.4 (q)	12.4 (q)	12.5 (q)	13.0 (q)	12.2 (t)	12.3 (q)
3-O-phenylacetyl													
1'	133.8 (s)	133.7 (s)	125.8 (s)	133.7 (s)	138.4 (s)	120.3 (s)	121.1 (s)	150.2 (s)	151.0 (s)	133.6 (s)		133.8 (s)	123.1 (s)
2'	129.4(d)	129.4(d)	130.6(d)	129.4(d)	126.5(d)	154.7 (s)	156.3 (s)	115.5(d)	117.6(d)	129.4 (s)		129.6(d)	155.3 (s)
3'	128.5(d)	128.5(d)	115.4(d)	128.5(d)	128.4(d)	117.4(d)	115.8(d)	125.5(d)	72.3 (d)	128.5(d)		128.9(d)	114.5(d)
4'	127.2(d)	127.2(d)	154.9 (s)	127.3(d)	128.7(d)	129.2(d)	129.1(d)	138.1(d)	72.2 (d)	127.3(d)		127.6(d)	129.2(d)
5'	128.5(d)	128.5(d)	115.4(d)	128.5(d)	128.4(d)	120.9(d)	120.1(d)	73.5 (d)	137.1(d)	128.5(d)		128.9(d)	122.5(d)
6'	129.4(d)	129.4(d)	130.6(d)	129.4(d)	126.5(d)	131.1(d)	132.3(d)	72.9 (d)	130.7(d)	129.4(d)		129.4(d)	131.2(d)
7'	41.53 (t)	41.5 (t)	40.6 (t)	41.5 (t)	72.8 (d)	37.3 (t)	36.4 (t)	38.5 (t)	32.4 (t)	41.5 (t)		41.5 (t)	36.4 (t)
8'	170.9(s)	170.9 (s)	171.3 (s)	170.9 (s)	173.7 (s)	172.1 (s)	171.7 (s)	165.8 (s)	165.8 (s)	170.9 (s)		169.9 (s)	172.0 (s)
5-OAc													
C=O	170.8(s)	170.7 (s)	170.8 (s)	170.7 (s)	170.8 (s)	171.2 (s)	170.9 (s)	170.6 (s)	170.7 (s)	170.8 (s)		171.0 (s)	171.1 (s)
CH ₃	21.0(q)	21.0 (q)	21.0 (q)	21.0 (q)	20.9 (q)	20.8 (q)	21.1 (q)	20.9 (q)	20.9 (q)	21.0 (q)		21.1 (q)	20.9 (q)
15-OAc													
C=O	169.6(s)	169.6 (s)	169.7 (s)	169.6 (s)	169.4 (s)	169.8 (s)	170.2 (s)	169.7 (s)	169.8 (s)	169.6 (s)			169.6 (s)
CH ₃	21.9 (s)	21.9 (q)	21.9 (q)	21.8 (q)	21.8 (q)	21.9 (q)	22.0 (q)	21.9 (q)	21.9 (q)	21.8 (q)			21.9 (q)
Glc													
1''													101.2(d)
2''													73.5 (d)
3''													75.9 (d)
4''													69.6 (d)
5''													75.9 (d)
6''													61.8 (t)

^a Measured at 125 MHz in CDCl₃. ^b Measured at 125 MHz in CD₃OD.

Metabolites **M1**, **M3**, and **M6** were detected at 8.49, 9.99, and 11.38 min, respectively. Taking **M1** as an example (Figure 4), the molecular ion at m/z 569.2746 ($[M + H]^+$) was observed, with a 16 Da mass shift attributed to an oxygen atom relative to the substrate euphorbiasteroid (**M0**). The fragment ions at m/z 509.2533 and m/z 449.2336 resulted from successive CH₃COOH loss from m/z 569.2746, and the fragment ions at m/z 433.2231, m/z 373.2012, and m/z 313.1801 were generated by C₆H₅CH₂COOH loss from the ions at m/z 569.2746, m/z 509.2533, and m/z 449.2336, respectively. Furthermore, the ion at m/z 313.1801 was fragmented to form ions at m/z 295.1697, m/z 277.1595 and m/z 267.1741 via loss of H₂O, 2H₂O and CO + H₂O, respectively. Moreover, the proposed fragmentation pathways of metabolites **M3** and **M6** were similar to those of metabolite **M1**, which were more likely to lose a H₂O group compared with **M0**. This clearly suggested that the hydroxylated site should be located on the methyl moiety of the molecule, but the exact substituted position remained to be determined.

Metabolites **M2**, **M4**, and **M5** were eluted at 9.79, 10.34, and 10.66 min. Taking **M2** as an example (Figure 4), the molecular ion at m/z 569.2748 ($[M + H]^+$) was observed, with a 16 Da mass shift attributed to an oxygen atom. The fragment ions at m/z 509.2543 and m/z 449.2332 resulted from successive CH₃COOH loss from the molecular ion at m/z 569.2748, and the fragment ions at m/z 375.2172 and m/z 315.1955 were generated by the loss of C₆H₅CHCOO from the ions at m/z 509.2543 and m/z 449.2332, respectively. In particular, the fragment ion at m/z 417.2275 resulted from the molecular ion at 569.2748 by losing C₆H₅CH₂COOH + O. Furthermore, the ion at m/z 315.1955 was fragmented to form ions at m/z 297.1854, m/z 279.1748, and m/z 269.1904 via loss of H₂O, 2H₂O, and CO + H₂O, respectively. Moreover, metabolites **M2**, **M4**, and **M5** were more likely to lose a H₂O group compared with euphorbiasteroid. The loss of C₆H₅CH₂COOH + O clearly suggested that the hydroxylated site should be located on the 3-O-phenylacetyl moiety of the molecule, but the exact substituted position remained to be determined.

Table 4. Mass spectrum characteristics of metabolites of euphorbiasteroid detected in vivo and in vitro.

No.	Component Name	RT (min)	Formula [M + H] ⁺	Observed <i>m/z</i>	Error (ppm)	MS ⁿ	Distribution				
							Rat			RLMs	Fungi
							Plasma	Urine	Faeces		
M1	M + O	8.49	C ₃₂ H ₄₁ O ₉	569.2746	0.18	569.2746, 509.2533, 449.2336, 433.2231, 373.2012, 355.1910, 313.1801, 295.1697, 277.1595, 267.1741, 249.1643	✓	✓	✓	✓	✓
M2	M + O	9.79	C ₃₂ H ₄₁ O ₉	569.2748	0.53	569.2748, 509.2543, 449.2332, 417.2275, 375.2172, 357.2069, 315.1955, 297.1854, 279.1748, 269.1904, 251.1803	-	✓	✓	✓	✓
M3	M + O	9.99	C ₃₂ H ₄₁ O ₉	569.2747	0.35	569.2747, 551.2642, 509.2538, 491.2438, 449.2336, 431.2226, 373.2020, 355.1910, 313.1805, 295.1699, 277.1592, 267.1745, 249.1645	✓	✓	✓	✓	✓
M4	M + O	10.34	C ₃₂ H ₄₁ O ₉	569.2756	1.93	569.2756, 509.2549, 449.2331, 417.2286, 375.2184, 357.2071, 315.1959, 297.1858, 279.1751, 269.1907, 251.1805	✓	✓	✓	✓	✓
M5	M + O	10.66	C ₃₂ H ₄₁ O ₉	569.2754	1.58	569.2754, 509.2547, 449.2329, 417.2288, 375.2181, 357.2071, 315.1959, 297.1865, 279.1751, 269.1912	✓	-	✓	✓	✓
M6	M + O	11.38	C ₃₂ H ₄₁ O ₉	569.2747	0.35	569.2747, 509.2542, 449.2339, 431.2230, 373.2020, 355.1910, 313.1806, 295.1699, 277.1592, 267.1745	✓	-	✓	✓	-
M7	M + 2O	6.06	C ₃₂ H ₄₁ O ₁₀	585.2688	-1.03	585.2688, 525.2480, 507.2377, 433.2221, 373.1995, 331.1906, 313.1796, 295.1701, 285.1841, 277.1594	✓	✓	-	✓	-
M8	M + 2O	6.36	C ₃₂ H ₄₁ O ₁₀	585.2704	1.71	585.2704, 525.2490, 507.2382, 465.2271, 433.2222, 391.2116, 373.2011, 355.1904, 313.1805, 295.1698, 285.1847, 267.1743, 255.1382	✓	✓	✓	✓	✓
M9	M + 2O	6.59	C ₃₂ H ₄₁ O ₁₀	585.2689	-0.85	585.2689, 525.2485, 507.2382, 465.2272, 447.2169, 433.2221, 391.2114, 373.2005, 355.1900, 313.1806, 295.1689, 285.1847, 277.1591, 267.1749	✓	✓	✓	✓	✓
M10	M + 2O	6.92	C ₃₂ H ₄₁ O ₁₀	585.2692	-0.34	585.2692, 525.2480, 507.2377, 465.2278, 391.2118, 373.2010, 355.1907, 313.1805, 295.1695, 267.1747	✓	-	✓	✓	-
M11	M + 2O	7.12	C ₃₂ H ₄₁ O ₁₀	585.2714	3.42	585.2714, 525.2496, 465.2284, 373.1997, 355.1906, 313.1802, 295.1706	✓	-	-	✓	-
M12	M + 2O + 2H	7.35	C ₃₂ H ₄₃ O ₁₀	587.2858	0.17	587.2858, 527.2645, 467.2433, 357.2069, 315.1961, 297.1860, 279.1752, 269.1905, 251.1796	✓	-	✓	✓	✓

Table 4. Cont.

No.	Component Name	RT (min)	Formula [M + H] ⁺	Observed <i>m/z</i>	Error (ppm)	MS ⁿ	Distribution				
							Rat			RLMs	Fungi
							Plasma	Urine	Faeces		
M13	M + 2O + 2H	7.49	C ₃₂ H ₄₃ O ₁₀	587.2867	2.72	587.2867, 527.2661, 509.2549, 467.2442, 449.2337, 417.2285, 357.2074, 315.1963, 297.1858, 279.1757, 269.1906	✓	-	✓	✓	✓
M14	M + O-2H	8.80	C ₃₂ H ₃₉ O ₉	567.2598	1.59	567.2598, 507.2377, 447.2166, 371.1853, 329.1760, 311.1644, 293.1538, 283.1700, 265.1597, 255.1747	✓	✓	✓	-	✓
M15	M + O-2H	8.95	C ₃₂ H ₃₉ O ₉	567.2598	1.59	567.2598, 507.2377, 447.2166, 371.1852, 329.1761, 311.1654, 293.1547, 283.1700, 265.1597	✓	✓	✓	-	-
M16	M + 2O-2H	8.71	C ₃₂ H ₃₉ O ₁₀	583.2530	-1.37	583.2530, 523.2330, 463.2126, 447.2032, 387.1815, 345.1707, 327.1595, 309.1498, 299.1645, 281.1541, 263.1438, 253.1591	✓	✓	✓	✓	✓
M17	M + 2O-2H	9.49	C ₃₂ H ₃₉ O ₁₀	583.2548	1.71	583.2548, 523.2332, 463.2132, 387.1814, 345.1710, 327.1600, 309.1490, 299.1647, 281.1540, 263.1449, 253.1596	✓	-	✓	✓	✓
M18	M + 3O-2H	5.96	C ₃₂ H ₃₉ O ₁₁	599.2497	1.67	599.2497, 539.2279, 387.1814, 345.1704, 327.1600, 309.1490, 299.1645, 281.1540, 263.1425, 253.1594	✓	✓	✓	-	-
M19	M + 3O-2H	6.37	C ₃₂ H ₃₉ O ₁₁	599.2505	3.00	599.2505, 539.2284, 479.2076, 447.2024, 405.1918, 387.1812, 345.1705, 327.1601, 309.1494, 299.1647, 281.1541, 263.1436, 253.1585	✓	✓	✓	✓	-
M20	M + 3O-2H	6.75	C ₃₂ H ₃₉ O ₁₁	599.2500	2.17	599.2500, 539.2286, 387.1811, 345.1711, 327.1602, 309.1496, 299.1648, 281.1547, 263.1438, 253.1591	✓	✓	✓	-	-
M21	M + 4O-2H	4.61	C ₃₂ H ₃₉ O ₁₂	615.2451	2.44	615.2451, 597.2335, 555.2226, 537.2123, 477.1913, 385.1654, 343.1542, 325.1440, 307.1334, 297.1497, 279.1386, 261.1280, 251.1426	✓	✓	✓	-	-
M22	M + 4O-2H	5.04	C ₃₂ H ₃₉ O ₁₂	615.2460	3.90	615.2460, 555.2236, 537.2133, 477.1919, 343.1549, 325.1448, 297.1494, 279.1389, 261.1285, 251.1437	✓	✓	✓	-	-
M23	M + 4O-2H	5.77	C ₃₂ H ₃₉ O ₁₂	615.2453	2.76	615.2453, 555.2231, 537.2125, 477.1916, 343.1549, 325.1440, 307.1335, 297.1493, 279.1390, 261.1286, 251.1439	✓	✓	✓	-	-
M24	M-2CH ₂ CO-C ₈ H ₆ O	5.84	C ₂₀ H ₃₁ O ₅	351.2166	0.00	351.2166, 333.2059, 315.1951, 297.1849, 279.1746, 269.1898, 251.1802	✓	✓	✓	✓	-

Table 4. Cont.

No.	Component Name	RT (min)	Formula [M + H] ⁺	Observed <i>m/z</i>	Error (ppm)	MS ⁿ	Distribution				
							Rat			RLMs	Fungi
							Plasma	Urine	Faeces		
M25	M-C ₂ H ₂ O	12.49	C ₃₀ H ₃₉ O ₇	511.2694	0.78	511.2694, 451.2482, 433.2373, 375.2171, 357.2068, 315.1959, 297.1858, 279.1750, 269.1902, 251.1431	✓	✓	✓	✓	-
M26	M-C ₂ H ₂ O + O	7.66	C ₃₀ H ₃₉ O ₈	527.2661	4.17	527.2661, 509.2540, 467.2440, 449.2337, 391.2120, 373.2017, 331.1910, 313.1803, 295.1696	✓	✓	✓	-	-
M27	M-C ₂ H ₂ O + O	9.14	C ₃₀ H ₃₉ O ₈	527.2647	1.52	527.2647, 509.2553, 467.2435, 449.2330, 391.2122, 373.2020, 331.1909, 313.1804, 295.1706	✓	✓	✓	-	✓
M28	M + O + C ₆ H ₁₀ O ₅	5.23	C ₃₈ H ₅₁ O ₁₄	731.3280	0.96	731.3280, 569.2768, 509.2549, 449.2335, 357.2074, 315.1971, 297.1868, 279.1754, 269.1911	-	-	✓	-	-
M29	M + O + C ₆ H ₁₀ O ₅	6.97	C ₃₈ H ₅₁ O ₁₄	731.3286	1.78	731.3286, 671.3065, 569.2745, 509.2544, 449.2331, 375.2173, 357.2073, 315.1963, 297.1855, 279.1752, 269.1902	✓	-	✓	-	✓
M30	M + 2O + SO ₃	2.87	C ₃₂ H ₄₁ O ₁₃ S	665.2271	1.35	665.2271, 647.2167, 605.2055, 587.1955, 545.1848, 393.1376, 313.1788, 295.1683, 277.1589, 267.1744	-	-	✓	-	-
M31	M + 2O + SO ₃	3.19	C ₃₂ H ₄₁ O ₁₃ S	665.2267	0.75	665.2267, 605.2061, 545.1843, 393.1371, 313.1805, 295.1691, 277.1580	-	-	✓	-	-

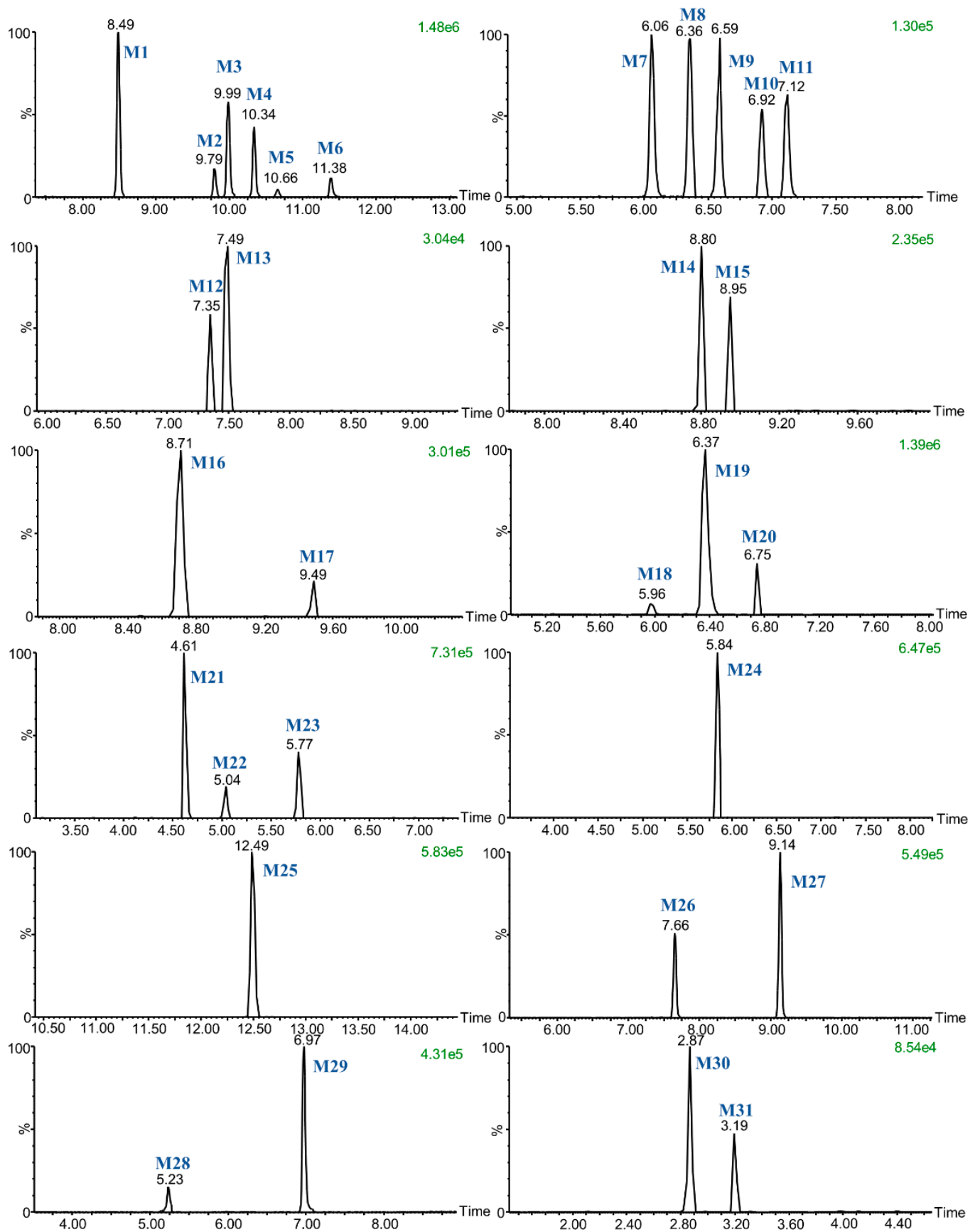


Figure 3. Extracted ion chromatograms of euphorbiasteroid metabolites in rats.

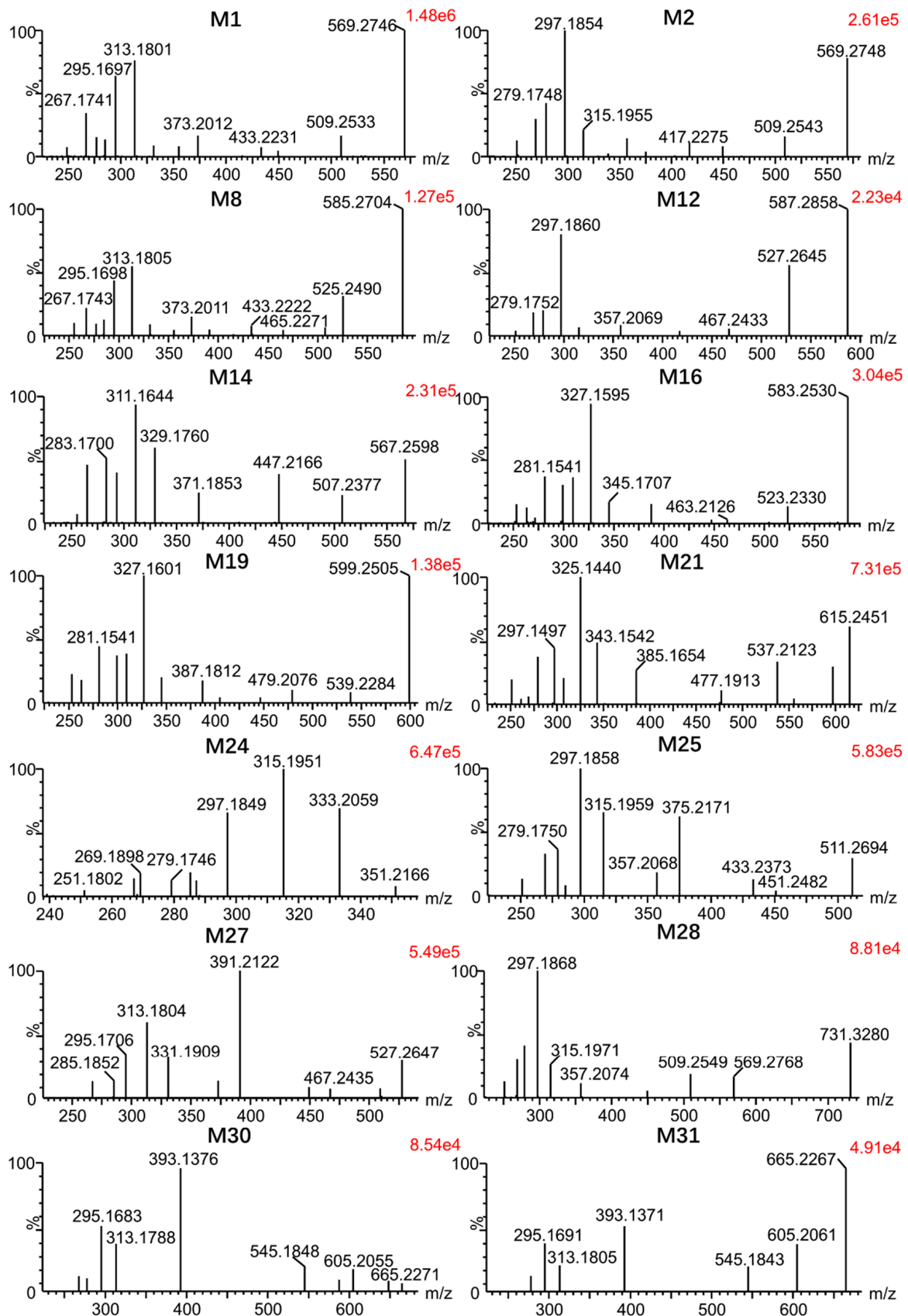


Figure 4. Product ion spectra of euphorbiasteroid metabolites in rats.

Metabolites **M7–M11** were predicted to be dihydroxylated derivatives with HPLC retention times at 6.06 and 7.12 min. For example, the molecular ion of **M8** was detected at m/z 585.2704 ($[M + H]^+$) in positive ion mode, 16 mass units more than those of **M1–M6**, suggesting the presence of an additional hydroxyl group (Figure 4). The fragment ions at m/z 525.2490 and m/z 465.2271 resulted from successive CH_3COOH loss of the parent ion at m/z 585.2704, and the ion at m/z 465.2271 was further fragmented to the ion at m/z 313.1805 by the loss of $\text{C}_6\text{H}_5\text{CH}_2\text{COOH} + \text{O}$, in which the ion at m/z 433.2222 resulted from m/z 585.2704 in a similar mechanism. The fragment ions at m/z 373.2011 and m/z 313.1805 were generated by successive CH_3COOH loss from the ion at m/z 433.2222. Furthermore, the ion at m/z 313.1805 was further fragmented to form the ions at m/z 295.1698 and m/z 285.1847 by the loss of H_2O and CO , respectively. Consistent with the monohydroxylated products of euphorbiasteroid, these showed a series of product ions resulting from the loss of CH_3COOH and $\text{C}_6\text{H}_5\text{CH}_2\text{COOH}$. This indicates that metabolites **M7–M11** may be produced by further hydroxylation on the basis of metabolites **M1–M6**.

Metabolites **M12** and **M13** were detected with HPLC retention times between 7.35 and 7.49 min. Taking **M12** as an example (Figure 4), the molecular ion at m/z 587.2858 ($[M + H]^+$) was observed, 34 Da higher than that of euphorbiasteroid. The fragment ions at m/z 527.2645 and m/z 467.2433 resulted from successive CH_3COOH loss of the parent ion at m/z 587.2858, and the ion at m/z 527.2645 was fragmented to the ion at m/z 357.2069 following the loss of $\text{C}_6\text{H}_5\text{CH}_2\text{COOH} + \text{H}_2\text{O} + \text{O}$. Furthermore, the fragment ion at m/z 297.1860 was formed via the elimination of CH_3COOH from the ion at m/z 357.2069, and the fragment ions at m/z 279.1752 and 269.1905 were produced by the loss of H_2O and CO from the ion at m/z 297.1860, respectively. The MS/MS spectra of **M12** and **M13** were similar to those of **M7–M11**, except that the corresponding ions were each heavier by 2 Da. Therefore, it was provisionally presumed that **M12** and **M13** were produced via changing the olefin of euphorbiasteroid into dihydrodiol.

The metabolites **M14** and **M15** were eluted between 8.80 and 8.95 min, and showed the protonated ion at m/z 567.2598 ($[M + H]^+$). They were 14 Da more than euphorbiasteroid and 2 Da less than **M1–M6** (Figure 4). Taking **M14** as an example, the fragment ions at m/z 507.2377 and m/z 447.2166 resulted from successive CH_3COOH loss from m/z 567.2598, while the fragment ions at m/z 371.1853 and m/z 311.1644 were formed via the elimination of $\text{C}_6\text{H}_5\text{CH}_2\text{COOH}$ from the ion at m/z 507.2377 and m/z 447.2166, respectively. Furthermore, the fragment ions at m/z 293.1538 and m/z 283.1700 also resulted from H_2O and CO loss from the ion at m/z 311.1644, respectively. In particular, the fragment ions at m/z 283.1700 and m/z 255.1747 were generated by successive loss of CO from the ion at m/z 311.1644, indicating the existence of an aldehyde group. Furthermore, according to the proposed metabolic pathway of tanshinone IIA [31], the methyl group of euphorbiasteroid might undergo similar metabolic modification, from methyl to primary alcohol, and then to an aldehyde group. Thus, it is provisionally interpreted that **M10** and **M11** were produced by transforming one methyl of euphorbiasteroid to aldehyde.

The metabolites **M16** and **M17**, which showed protonated molecular ions at m/z 583.2530 ($[M + H]^+$) with the retention times of 8.71 and 9.49 min, were 30 Da higher than euphorbiasteroid and 2 Da less than the dihydroxylation products of euphorbiasteroid like **M7–M11** (Figure 4). Taking **M16** as an example, the fragment ions at m/z 523.2330 and m/z 463.2126 were proposed to result from successive loss of CH_3COOH from the molecular ion m/z 583.2530. In addition, the fragment ions at m/z 447.2032, m/z 387.1815, and m/z 327.1595 were generated from the ions at m/z 583.2530, m/z 523.2330 and m/z 463.2126 through the loss of $\text{C}_6\text{H}_5\text{CH}_2\text{COOH}$, respectively. The ion at m/z 327.1595 was further fragmented into the ions at m/z 309.1498 and m/z 299.1645 via the loss of H_2O and CO , respectively. In particular, the fragment ions at m/z 281.1541, m/z 263.1438, and m/z 253.1591 were formed via the elimination of HCOOH from the ions at m/z 327.1595, m/z 309.1498, and m/z 299.1645, respectively, which indicated the existence of a carboxyl group. The compounds might be produced by the oxidation of **M14** or **M15**, which was consistent

with our initial speculation. Thus, it is provisionally interpreted that **M16** and **M17** were produced by oxidizing the aldehyde of **M14** or **M15** into carboxyl groups.

Metabolites (**M18–M20**) were detected between 5.96 and 6.75 min. Taking **M19** as an example (Figure 4), it showed a molecular ion at m/z 599.2505 ($[M + H]^+$), with 16 Da higher than the metabolites **M16** and **M17**. The fragment ions at m/z 539.2284 and m/z 479.2076 resulted from successive CH_3COOH loss from the parent ion at m/z 599.2505, while the fragment ions at m/z 447.2024, m/z 387.1812, and m/z 327.1601 were proposed to result from loss of $\text{C}_6\text{H}_5\text{CH}_2\text{COOH} + \text{O}$ from the ions at m/z 599.2505, m/z 539.2284, and m/z 479.2076, respectively. Additionally, a battery of fragment ions at m/z 309.1494, m/z 299.1647, m/z 281.1541, m/z 263.1436 and m/z 253.1585 were produced, which were consistent with the fragmentation behaviors of the metabolites **M16** and **M17**. Therefore, these metabolites were provisionally characterized as monohydroxylated products of the metabolites **M16** and **M17**.

The metabolites (**M21–M23**) were eluted at between 4.61 and 5.77 min, giving rise to the protonated molecules $[M + H]^+$ at m/z 615.2451. Taking **M21** as an example (Figure 4), the fragment ion at m/z 615.2451 was fragmented into the ions at m/z 555.2226, m/z 537.2123, and m/z 477.1913 following the loss of CH_3COOH , $\text{CH}_3\text{COOH} + \text{H}_2\text{O}$, and $2\text{CH}_3\text{COOH} + \text{H}_2\text{O}$, respectively. The fragment ions at m/z 385.1654 and m/z 325.1440 were proposed to result from loss of $\text{C}_6\text{H}_5\text{CH}_2\text{COOH} + \text{O}$ from the ions at m/z 537.2123 and m/z 477.1913, respectively. In particular, the MS/MS characteristic ions of the metabolite **M21** (m/z 385.1654, 325.1440, 307.1334, 297.1497, 279.1386, 261.1280, and 251.1426) were 2 Da less than those of the metabolites **M16** and **M17**. Therefore, they were tentatively identified as dihydroxylated products of metabolites **M16** and **M17**.

The metabolite **M24** was observed as its protonated molecular ion $[M + H]^+$ at m/z 351.2166 with a retention time of 5.84 min, which was deductively assigned as a hydrolysis product of euphorbiasteroid because its protonated ion was 202 Da less than that of euphorbiasteroid (Figure 4). The fragment ions at m/z 333.2059, m/z 315.1951, m/z 297.1849, and m/z 279.1746 resulted from successive H_2O loss from the parent ion at m/z 351.2166. Furthermore, a battery of fragment ions at m/z 315.1951, m/z 297.1849, m/z 279.1746, m/z 269.1898, and m/z 251.1802 were produced, which were consistent with fragmentation behaviors of euphorbiasteroid. Therefore, the metabolite **M24** was probably formed via the loss of two CH_2CO and a $\text{C}_6\text{H}_5\text{CHCO}$ from the prototype compound euphorbiasteroid. Similar findings have been reported before [32].

The metabolite **M25** provided its protonated ion at m/z 511.2694 with a retention time of 12.49 min (Figure 4). It was 42 Da less than that of euphorbiasteroid, meaning that it might be a hydrolysis product of euphorbiasteroid. In the MS/MS spectrum, a battery of fragment ions at m/z 451.2482 $[M + \text{H}-\text{CH}_3\text{COOH}]^+$, m/z 433.2373 $[M + \text{H}-\text{CH}_3\text{COOH}-\text{H}_2\text{O}]^+$, m/z 375.2171 $[M + \text{H}-\text{C}_6\text{H}_5\text{CH}_2\text{COOH}]^+$, and m/z 297.1858 $[M + \text{H}-\text{CH}_3\text{COOH}-\text{H}_2\text{O}-\text{C}_6\text{H}_5\text{CH}_2\text{COOH}]^+$ were observed, suggesting that the metabolite **M25** was produced by losing an acetyl of euphorbiasteroid.

The metabolites **M26** and **M27**, which showed their respective positive ions at m/z 527.2661 and 527.2647 with the retention times of 7.66 and 9.14 min, were plausibly assigned as monohydroxylated products of metabolite **M25** due to their protonated ions being 16 Da more than that of **M25** (Figure 4). In the MS/MS spectrum of **M27**, the characteristic fragment ions at m/z 467.2435 $[M + \text{H}-\text{CH}_3\text{COOH}]^+$, m/z 391.2122 $[M + \text{H}-\text{C}_6\text{H}_5\text{CH}_2\text{COOH}]^+$, and m/z 331.1909 $[M + \text{H}-\text{CH}_3\text{COOH}-\text{C}_6\text{H}_5\text{CH}_2\text{COOH}]^+$ were detected, which was in accordance with the mass fragmentation behaviors of **M25**. In addition, the fragment ions at m/z 313.1804 $[M + \text{H}-\text{CH}_3\text{COOH}-\text{C}_6\text{H}_5\text{CH}_2\text{COOH}-\text{H}_2\text{O}]^+$ and m/z 295.1706 $[M + \text{H}-\text{CH}_3\text{COOH}-\text{C}_6\text{H}_5\text{CH}_2\text{COOH}-2\text{H}_2\text{O}]^+$ proved the existence of hydroxylation. According to the reliable analysis above, they were provisionally characterized as monohydroxylated products of **M25**.

The metabolites **M28** and **M29** gave rise to protonated ions at m/z 731.3280 and 731.3286, which were eluted at 5.23 and 6.97 min, respectively. They were 162 Da more than metabolites **M1–M6**. Taking **M28** as an example (Figure 4), the fragment ion at

m/z 569.2768 provided reliable evidence for identifying the metabolites as glycosylation products of euphorbiasteroid due to the loss of 162 mass units. The fragment ions at m/z 509.2549, 449.2335, 357.2074, 315.1971, 297.1868, 279.1754, and 269.1917 demonstrated that a hydroxyl group in the metabolites **M7–M11** was replaced by $C_6H_{10}O_5$. Therefore, they were tentatively identified as glycosylation products of euphorbiasteroid.

The metabolites **M30** and **M31** were observed with their protonated ions at m/z 665.2271 and 665.2267 with retention times of 2.87 and 3.19 min, which were deductively assigned as sulfonated products of the metabolites **M7–M11** because their protonated ions were 80 Da larger than the metabolites **M7–M11** (Figure 4). In the MS/MS spectrum of **M30**, the characteristic ions at m/z 605.2055 $[M + H-CH_3COOH]^+$, m/z 545.1848 $[M + H-2CH_3COOH]^+$, and m/z 393.1376 $[M + H-2CH_3COOH-C_6H_5CH_2COOH-O]^+$ were consistent with fragmentation characteristics of euphorbiasteroid, which provided reliable reference for the identification of **M30**. Particularly, the fragment ion at m/z 313.1788 was proposed to result from the loss of SO_3 from the ion at m/z 393.1376. Moreover, a battery of fragment ions at m/z 295.1683, m/z 277.1589, and m/z 267.1744 were also observed, suggesting that the metabolites **M30** and **M31** should be sulfonated products of metabolites **M7–M11**.

Finally, in order to explore whether RLMs and the microbial model could simulate the metabolism of euphorbiasteroid in rats, the incubation of RLMs and *C. elegans* bio-110930 with euphorbiasteroid were studied, respectively. The results showed that 18 and 14 metabolites identified in the above two models could match those of rats in vivo, respectively, indicating that they could simulate the metabolism of euphorbiasteroid in vivo to a certain extent. Considering the economic benefits and transformation efficiency, the large-scale microbial transformation experiment was used for the subsequent preparation of metabolite standards and the accurate characterization of the metabolite structures [33–35].

3.3. The Structure Elucidation of Transformation Products

Through large-scale microbial transformation and chemical hydrolysis experiments, twelve transformation products (**1–12**) were prepared, including eleven new compounds (**1–9**, **11** and **12**) and one known compound (**10**). Compound **10** was characterized as epoxythyrol by comparison of the NMR and HR-ESI-MS data with the literature [36]. The structures of eleven new transformation products were characterized by ESI-MS, HR-ESI-MS, 1D-, and 2D-NMR data (Figure 5).

Compound **1** was isolated as a white powder with an optical rotation of $[\alpha]_D^{20} +116.10^\circ$ (c 0.118, MeOH). The molecular formula of $C_{32}H_{40}O_9$ was deduced from the $[M + H]^+$ ion at m/z 569.2746, and the molecular weight of compound **1** is 16 Da more than that of the precursor compound euphorbiasteroid. Analysis of the 1H and ^{13}C NMR spectroscopic data of **1** revealed its structural similarity to euphorbiasteroid (**M0**, Tables 1 and 3). The only difference between these two compounds was the occurrence of an extra hydroxymethyl [δ_C 71.2, δ_H 3.52 (d, $J = 11.25$ Hz, H-18a)] and δ_H 3.44 (d, $J = 11.25$ Hz, H-18b)) in compound **1**, taking the place of a methyl of euphorbiasteroid. In the HMBC spectrum of compound **1**, the two protons of hydroxymethyl at δ_H 3.52 and 3.44 exhibited long-range HMBC correlations with C-9 (δ_C 30.2) and C-11 (δ_C 25.2) (Figure 6), suggesting that a hydroxyl might be substituted at C-18 or C-19 position. In the NOESY spectrum (Figure 7), the key NOE correlations of two hydroxymethyl protons (δ_H 3.52 and 3.44) with H-9 (δ_H 1.21) and H-11 (δ_H 1.65) proved that the C-18 of compound **1** was substituted by a hydroxyl, and assigned the relative configuration of 18-hydroxymethyl to be α -oriented. Unambiguous complete assignments for the 1H and ^{13}C NMR signals were made by combination of DEPT, 1H - 1H COSY, HSQC, HMBC, and NOESY spectra (Figures S1–S10). On the basis of the above evidence, the structure of compound **1** was thus established as 18 α -hydroxyl euphorbiasteroid.

Compound **2** was isolated as a white powder with $[\alpha]_D^{20} +74.89^\circ$ (c 0.150, MeOH). The molecular formula was assigned as $C_{32}H_{40}O_9$ based on its HR-ESI-MS data that displayed an $[M + H]^+$ ion at m/z 569.2747. Similar to compound **1**, the molecular weight of **2** was 16 mass units more than that of euphorbiasteroid and shared the same molecular formula.

The ^1H and ^{13}C NMR data of compound **2** were quite close to those of euphorbiasteroid (Tables 1 and 3), except for the absence of an aromatic proton. In the ^1H NMR spectrum of **1**, two groups of aromatic protons (each two protons) supported the presence of a *p*-substituted benzyl ring. Two groups of carbon resonances (each two carbons) at δ_{C} 130.6 and 115.4 as well as the ^{13}C chemical shift of C-4' proved the above deduction, and attributed a hydroxyl substitution at C-4' (Figures S11–S20). On the basis of the above evidence, the structure of compound **2** was established as 4'-hydroxyl euphorbiasteroid.

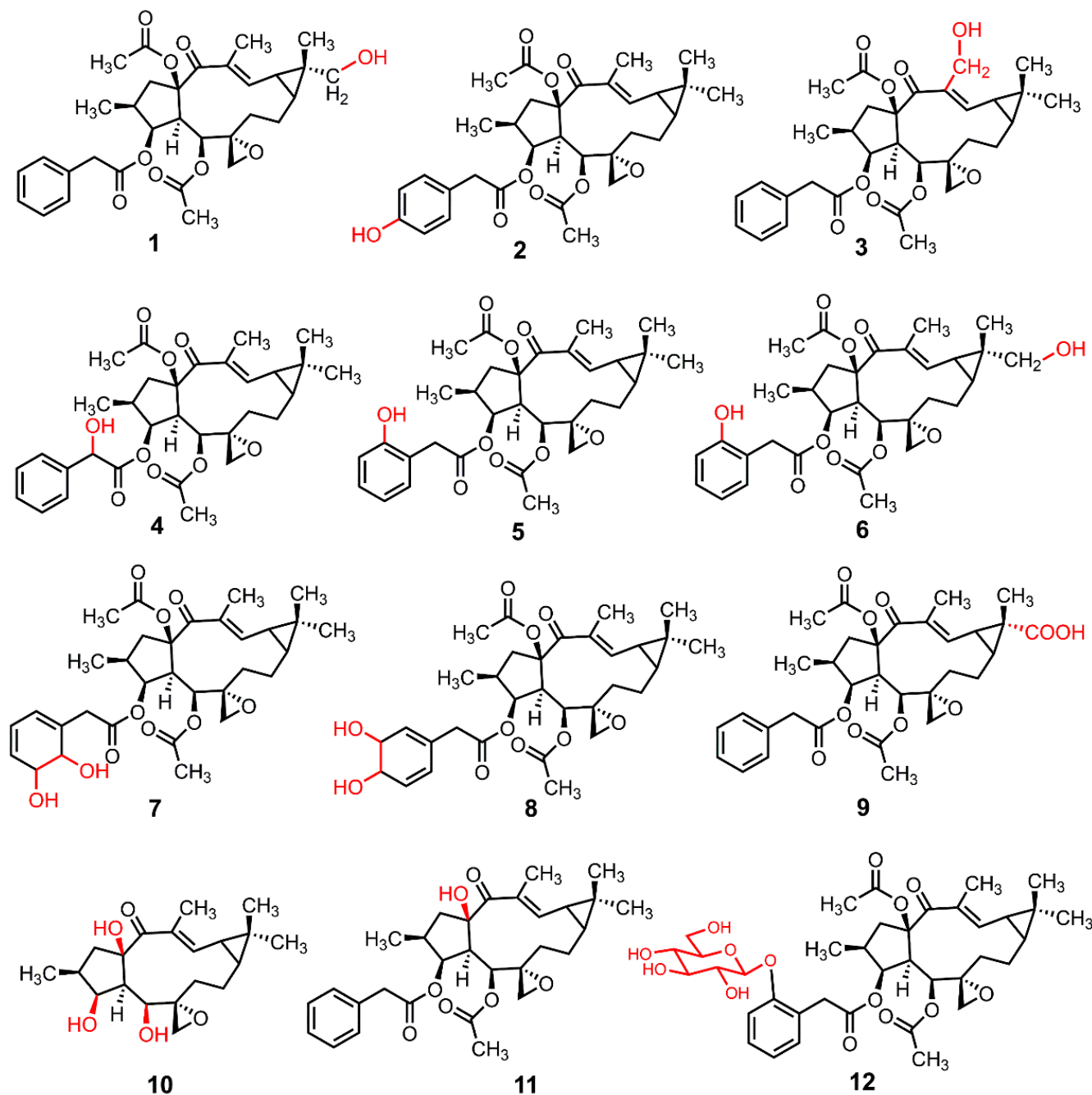


Figure 5. The structures of euphorbiasteroid and its transformation products.

Compound **3**, a white powder, had an optical rotation of $[\alpha]_{\text{D}}^{20} +63.97^\circ$ (c 0.130, MeOH). Its molecular formula was deduced to be $\text{C}_{32}\text{H}_{40}\text{O}_9$ from the $[\text{M} + \text{H}]^+$ ion at m/z 569.2746 in HRESIMS. Compound **3** was proposed to be a hydroxylated product of euphorbiasteroid due to its molecular weight being 16 mass units more than that of euphorbiasteroid. When comparing its ^1H and ^{13}C NMR data with those of euphorbiasteroid (Tables 1 and 3), it

was revealed that the two compounds shared a great similarity. In the NMR spectra, the appearance of an extra oxygenated methylene unit [δ_{H} 4.28 (d, $J = 12.38$ Hz, H-20a) and δ_{H} 4.42 (d, $J = 12.38$ Hz, H-20b); δ_{C} 58.1], in place of the methyl signals for C-20 (δ_{H} 1.82; δ_{C} 12.3) in euphorbiasteroid, suggested that one hydroxyl was incorporated to **3** at C-20 position. Key HMBC correlations of two protons of the hydroxymethyl (δ_{H} 4.28 and 4.42) with C-14 (δ_{C} 198.4) and C-12 (δ_{C} 147.6) attached a hydroxyl to C-20 (Figure 6). Assignments of the ^1H and ^{13}C NMR signals were achieved by a combination of DEPT, ^1H - ^1H COSY, HSQC, and HMBC experiments (Figures S21–S30). Thus, the structure of compound **3** was identified as 20-hydroxyl euphorbiasteroid.

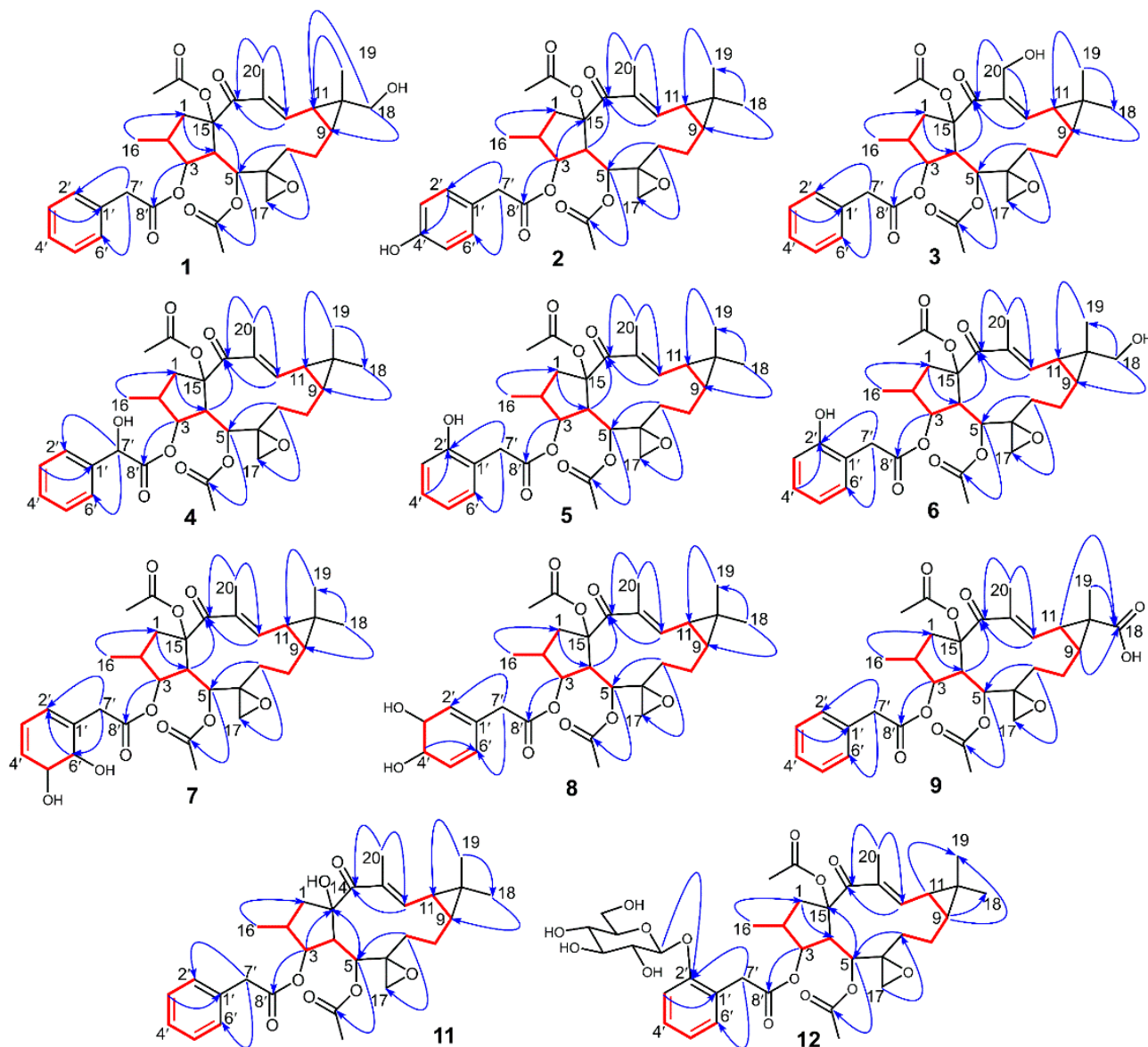


Figure 6. ^1H - ^1H COSY (—) and HMBC (→) correlations of compounds **1–9** and **11–12**.

Compound **4** was obtained as a white powder with $[\alpha]_{\text{D}}^{20} +70.00^\circ$ (c 0.125, MeOH). The protonated ion $[\text{M} + \text{H}]^+$ at m/z 569.2756 (calcd for $\text{C}_{32}\text{H}_{41}\text{O}_9$, 569.2745) in HRESIMS assigned the molecular formula to be $\text{C}_{32}\text{H}_{40}\text{O}_9$. The ^1H and ^{13}C NMR data of **4** closely matched those of euphorbiasteroid (Tables 1 and 3). The only difference was the appearance of the signals for an oxygenated methine (δ_{H} 5.10, δ_{C} 72.8) in **4**, rather than the C-7' methylene signals (δ_{H} 3.58, δ_{C} 41.5). Thus, it was speculated that compound **4** was a C-7' hydroxylated product of euphorbiasteroid. In addition, relative to euphorbiasteroid, the chemical shifts of C-1' and C-8' of compound **4** were downfield shifted significantly from

δ_C 133.8 to δ_C 138.4, and from δ_C 170.9 to δ_C 173.7, respectively, while the resonances of C-2' and C-6' was upfield shifted from δ_C 129.4 to δ_C 126.5. The key HMBC correlations from H-7' at δ_H 5.10 to C-1', C-2', C-6' and C-8' (Figure 6) further proved that a hydroxyl was substituted at C-7' position. The stereo configuration of 7'-OH failed to be determined due to a lack of substantial NOE correlation (Figures S31–S40). Therefore, compound 4 was assigned as 7'-hydroxyl euphorbiasteroid.

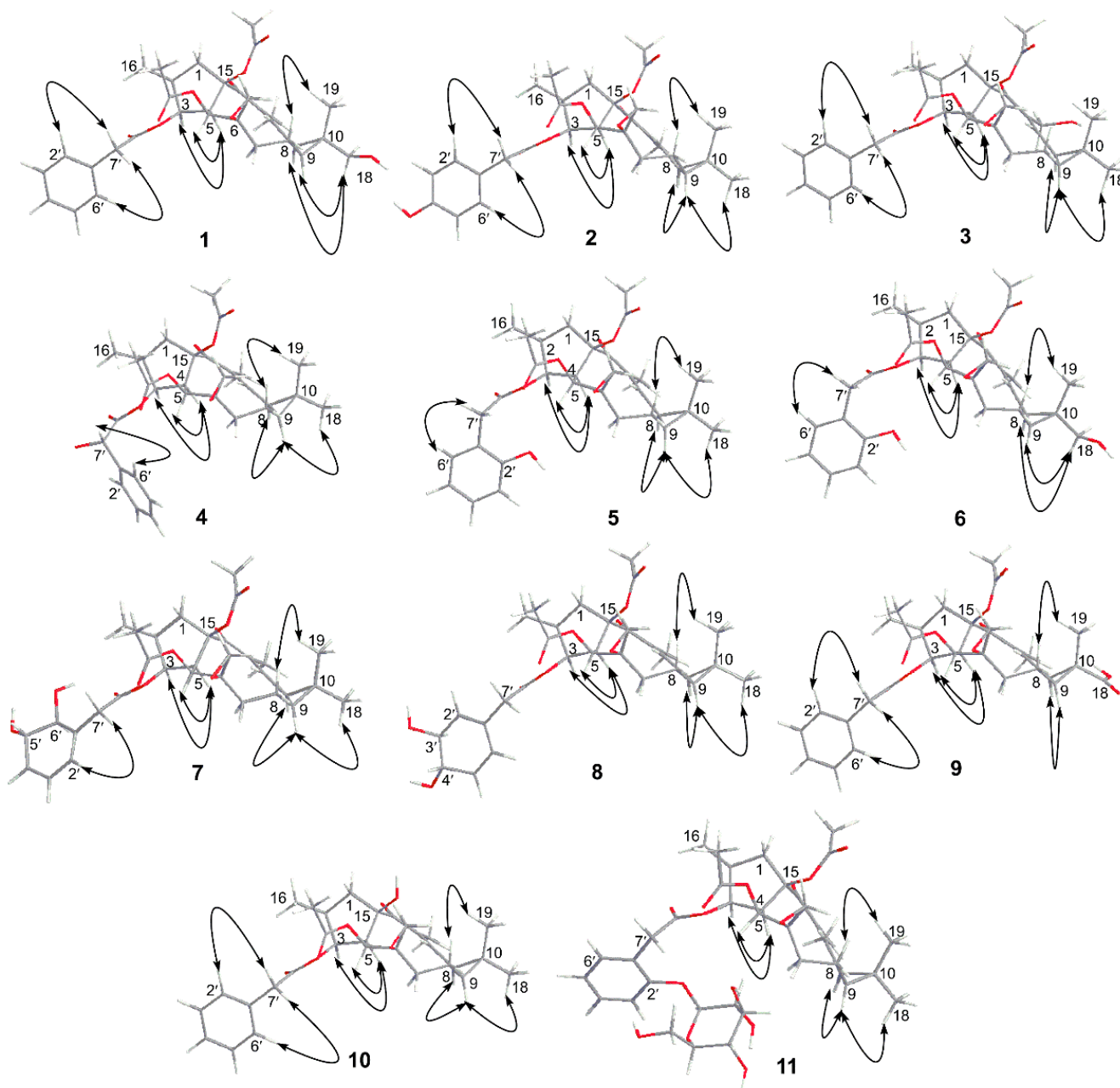


Figure 7. NOESY (↔) correlations of compounds 1–9 and 11–12.

Compound 5 was isolated as a white powder with the optical rotation $[\alpha]_D^{20} +112.65^\circ$ (c 0.108, MeOH). The molecular formula was inferred as $C_{32}H_{40}O_9$ due to the appearance of an $[M + H]^+$ ion at m/z 569.2754 in the HR-ESI-MS spectrum. In the 1H and ^{13}C NMR spectra of 5 (Tables 1 and 3), compared to euphorbiasteroid, it was observed to have one additional oxygenated quaternary carbon at δ_C 154.7, replacing an aromatic methine of the benzyl ring. Additionally, the 1H NMR spectrum exhibited four aromatic proton signals for an AA'BB' coupling system at δ_H 6.90, 7.18, 6.88, and 7.11. The above information, in

combination with key HMBC correlations from H₂-7' (δ_{H} 3.70 and 3.55) to C-2' (δ_{C} 154.7) and C-6' (δ_{C} 131.1), supported that a hydroxyl was substituted at the C-2' of the benzyl ring. Unambiguously complete assignments for the ¹H and ¹³C NMR signals were made by a combination of DEPT, ¹H-¹H COSY, HSQC, and HMBC spectra (Figures S41–S50). Thus, compound **5** was identified as 2'-hydroxyl euphorbiasteroid.

The molecular formula of compound **6** was deduced to be C₃₂H₄₀O₁₀ from the HR-ESI-MS [M + H]⁺ ion *m/z* 585.2704 (calcd for C₃₂H₄₁O₁₀, 585.2694). Its molecular weight was 16 mass units more than that of compound **5**, implying that compound **6** might be a dihydroxylated product of euphorbiasteroid. The ¹H and ¹³C NMR data closely resembled those of **5** (Figures S51–S60). The only difference was that compound **6** had an extra hydroxymethyl (δ_{H} 3.48, 3.38; δ_{C} 70.9), instead of a methyl (δ_{H} 1.20; δ_{C} 28.9) of **5**. In the HMBC spectrum (Figure 6), key long-range correlations from two hydroxymethylene protons at δ_{H} 3.48 and 3.38 to C-9 (δ_{C} 31.1) and C-11 (δ_{C} 26.2) revealed that a hydroxyl was linked to C-18 or C-19 position. The observation of NOE correlations (Figure 7) from the hydroxymethylene protons at δ_{H} 3.48 and 3.38 to H-9 (δ_{H} 1.33) and H-11 (δ_{H} 1.78) unambiguously attributed the hydroxymethylene as C-18, and determined the relative configuration of 18-CH₂OH to be α -oriented. Therefore, the chemical structure of compound **6** was identified as 18 α , 2'-dihydroxyl euphorbiasteroid.

Compound **7** was obtained as a white powder with an optical rotation $[\alpha]_{\text{D}}^{20} +60.00^{\circ}$ (*c* 0.170, MeOH). Its molecular formula was deduced as C₃₂H₄₂O₁₀ due to the [M + H]⁺ ion at *m/z* 587.2851 (calcd for C₃₂H₄₃O₁₀, 587.2878) in HR-ESI-MS. Interestingly, the molecular weight of **7** was 34 mass units more than that of euphorbiasteroid, and had one less degree of unsaturation, suggesting that there was a possible missing double bond or ring as well as two hydroxyl substituents. The ¹H and ¹³C NMR spectroscopic data (Tables 2 and 3) showed that compound **7** shared most of its featured functionalities and had the same diterpene skeleton as euphorbiasteroid, but had a great difference in the phenylacetyl moiety. Only three aromatic proton signals occurred at δ_{H} 5.54, 7.54, and 6.07 in the ¹H NMR spectrum, and four aromatic carbon resonances were observed at δ_{C} 150.2, 115.5, 125.5, and 138.1 in the ¹³C NMR spectrum. Detailed interpretation of the NMR spectroscopic data indicated that two additional oxygenated aliphatic methines [δ_{H} 4.26 (d, *J* = 7.49 Hz), 3.76 (m); δ_{C} 73.5, 72.9] in compound **7** replaced two aromatic methines [δ_{H} 7.30 (m), 7.25 (overlap); δ_{C} 128.5, 129.4] of euphorbiasteroid. The ¹H-¹H COSY correlations of H-2' (δ_{H} 5.54)/H-3' (δ_{H} 7.54)/H-4' (δ_{H} 6.07)/H-5' (δ_{H} 4.26)/H-6' (δ_{H} 3.76) in combination with the key HMBC long-range correlations from H₂-7' (δ_{H} 2.67, 2.54) to C-2' (δ_{C} 115.5) and C-6' (δ_{C} 72.9) (Figure 6) evidenced that the C-5' and C-6' double bond of phenyl ring was hydrogenated and subsequently substituted by two hydroxyls, which was in agreement with the molecular weight and degrees of unsaturation of **7** as mentioned above. The stereo configurations of 5'-OH and 6'-OH failed to be determined due to a lack of substantial NOE correlations in the NOESY spectrum of compound **7** (Figures S61–S70). Based on the above analysis, the chemical structure of compound **7** was identified as 5',6'-dihydroxyl dihydroeuphorbiasteroid.

Compound **8**, a yellowish powder with $[\alpha]_{\text{D}}^{20} +90.83^{\circ}$ (*c* 0.123, MeOH), had the same molecular formula C₃₂H₄₂O₁₀ and degrees of unsaturation as compound **7** due to the [M + H]⁺ ion peak at *m/z* 587.2873 (calcd for C₃₂H₄₃O₁₀, 587.2878) in its HR-ESI-MS spectrum. The ¹H and ¹³C NMR spectra (Tables 2 and 3) demonstrated almost the same spectroscopic features as those of compound **7**, including a diterpenoid skeleton, two acetyl moieties, and a hydrogenated and dihydroxylated phenyl acetyl moiety [δ_{H} 5.66 (s), 3.72 (brs), 4.25 (brd., 5.56), 6.07, 6.15 (d, *J* = 10.14 Hz), 3.69, and 2.55; δ_{C} 151.0, 117.6, 72.3, 72.2, 137.1, 130.732.4, and 165.8], suggesting that compounds **7** and **8** might be isomers. Detailed analysis of the ¹H and ¹³C NMR spectroscopic data revealed that compound **8** had a different hydrogenated and dihydroxylated position. In 2D NMR spectra, the ¹H-¹H COSY correlations of H-2' (δ_{H} 5.66)/H-3' (δ_{H} 3.72)/H-4' (δ_{H} 4.25)/H-5' (δ_{H} 6.07)/H-6' (δ_{H} 6.15) implied that the C-3' and C-4' double bond of phenyl ring was hydrogenated and subsequently substituted by two hydroxyls, respectively. The above deduction was further

proved by key HMBC correlations of H₂-7' (δ_{H} 3.69, 2.55) with the aromatic C-2' (δ_{C} 117.6) and C-6' (δ_{C} 130.7), and of H-4' [δ_{H} 5.66 (brd., $J = 5.56$ Hz)] with C-6' (Figures S71–S80). Thus, the structure of compound **8** was identified as 3',4'-dihydroxyl dihydroeuphorbiasteroid. The stereo configurations of 3'-OH and 4'-OH failed to be determined due to a lack of substantial NOE correlations.

Compound **9** was isolated as a white powder with an optical rotation of $[\alpha]_{\text{D}}^{20} +77.78^{\circ}$ (c 0.123, MeOH). The HREI-MS exhibited the $[\text{M} + \text{H}]^{+}$ ion at m/z 583.2330 (calcd. 583.2543), corresponding to the molecular formula C₃₂H₃₈O₁₀. The molecular weight of **9** was 30 mass units more than that of the substrate euphorbiasteroid, implying that compound **9** might be a carboxylated product. Compared to the substrate euphorbiasteroid, the ¹H and ¹³C NMR spectra (Tables 2 and 3) exhibited an additional carboxyl signal (δ_{C} 179.8), but an absence of the signals for CH₃-18 (δ_{H} 1.20; δ_{C} 28.9). Additionally, the chemical shift of C-19 was significantly shifted to high field by 6.4 ppm. These data implied that compound **9** might be a C-18 carboxylated product of euphorbiasteroid. This deduction was substantially proved by key HMBC correlations (Figure 6) from CH₃-19 (δ_{H} 1.44), H-9 (δ_{H} 1.90), and H-11 (δ_{H} 2.44) to the carboxyl carbon (δ_{C} 179.8) (Figure S81–S90). Thus, the structure of compound **9** was thus identified as 18 α -carboxyl euphorbiasteroid.

Compound **11** was isolated as a white powder with $[\alpha]_{\text{D}}^{20} +117.01^{\circ}$ (c 0.146, MeOH). Its HR-ESI-MS spectrum gave a hydrogen adduct ion at m/z 511.2694, assigning the molecular formula of **11** as C₃₀H₃₈O₇. The ¹H and ¹³C NMR spectra of **11** exhibited quite similar spectroscopic features to those of **M0**, including four methyls [δ_{H} 0.81 (d, $J = 6.69$ Hz), 1.21 (s), 1.25 (s), 1.78 (s); δ_{C} 14.2, 29.0, 16.3, 12.2], one double bond [δ_{H} 7.32 (overlap), δ_{C} 150.8, 135.1], one ketone carbonyl (δ_{C} 199.3), one acetoxyl [δ_{H} 2.08 (3H, s), δ_{C} 171.0, 21.1], one oxygenated methine (δ_{H} 5.46; δ_{C} 82.8), and one oxygenated quaternary carbon (δ_{C} 88.7), and one characteristic three-membered epoxy motif (δ_{H} 2.41 and 2.27, δ_{C} 58.9 and 55.4), with the exception of the disappearance of one acetoxyl in **11** (Tables 2 and 3). The downfield shifted carbon signals at C-1 ($\Delta\delta$ +2.0)/C-4 ($\Delta\delta$ +1.7)/C-5 ($\Delta\delta$ +0.8)/C-14 ($\Delta\delta$ +2.4) and the upfield shifted C-15 ($\Delta\delta$ -3.0) suggested that the acetoxyl at C-15 was replaced by one hydroxyl. Furthermore, the key HMBC correlations from the protons at δ_{H} 5.92 (H-5) and 5.46 (H-3) to C-15 (δ_{C} 88.7) further supported the above deduction (Figure 6). Interpretation of the NOESY spectrum revealed that compound **11** shared the same relative configurations as those of **M0** (Figure 7). Therefore, the structure of compound **11** was identified as 15-deacetyl euphorbiasteroid (Figures S94–S103).

The HR-ESI-MS spectrum of compound **12** gave a hydrogen adduct ion $[\text{M} + \text{H}]^{+}$ m/z 731.3280 (calcd for C₃₈H₅₀O₁₄, 731.3273), assigning the molecular formula as C₃₈H₅₀O₁₄. Its molecular weight was 162 Da more than that of the substrate euphorbiasteroid, implying that compound **12** might be a hexosylated product of euphorbiasteroid. The ¹H and ¹³C NMR spectroscopic data of compound **12** were very similar to those of the substrate euphorbiasteroid, and the major difference was the presence of an additional glucosyl unit [δ_{H} 4.81 and 3.49–3.89 (6H); δ_{C} 101.4, 75.9, 75.9, 73.5, 69.6, 61.8] in the structure of **12** (Tables 2 and 3). The substitution position of glucosyl was unambiguously determined to be the C-2' of the phenyl ring due to key HMBC correlations from the anomeric proton (δ_{H} 4.81) of glucosyl and H₂-7' (δ_{H} 3.67, 3.64) to C-2' (δ_{C} 155.3) (Figure 6). The ¹³C chemical shifts of glucosyl and the large coupling constant of the anomeric proton ($J_{\text{H-1}''/\text{H-2}''} = 6.77$ Hz) attributed the glucosyl to be β -D-glucose. Assignment of the ¹H and ¹³C NMR signals was achieved by a combination of DEPT, ¹H-¹H COSY, and HSQC experiments (Figure S104–S113). Based on this evidence, the structure of compound **12** was determined to be euphorbiasteroid 2'-O- β -D-glucopyranoside.

3.4. Comparison of Metabolite Formation In Vitro and In Vivo

Various results of metabolite formation were discovered in the three approaches used in this study. Rat plasma, urine, and feces samples were generally rich in metabolites, with 27, 20, and 29 metabolites, respectively. In vitro incubation of RLMs produced the same 18 phase I metabolites as the metabolites in rats, just less in number and amount. In vitro

co-incubation of *C. elegans* bio-110930 with euphorbiasteroid yielded 14 metabolites, 12 of which were further prepared by large scale microbial transformation and confirmed to be the same metabolites as those in rats by comparison of their HPLC retention times and MS/MS fragments (Figure 8). On the basis of analysis of 1D and 2D NMR spectroscopic data, 12 metabolites were identified as 18 α -hydroxyl euphorbiasteroid (M1), 4'-hydroxyl euphorbiasteroid (M2), 20-hydroxyl euphorbiasteroid (M3), 7'-hydroxyl euphorbiasteroid (M4), 2'-hydroxyl euphorbiasteroid (M5), 18 α ,2'-dihydroxyl euphorbiasteroid (M8), 5',6'-dihydroxyl dihydroeuphorbiasteroid (M12), 3',4'-dihydroxyl dihydroeuphorbiasteroid (M13), 18 α -carboxyl euphorbiasteroid (M16), epoxyathyrol (M24), 15-deacetyl euphorbiasteroid (M25), and euphorbiasteroid 2'-O- β -D-glucopyranoside (M29).

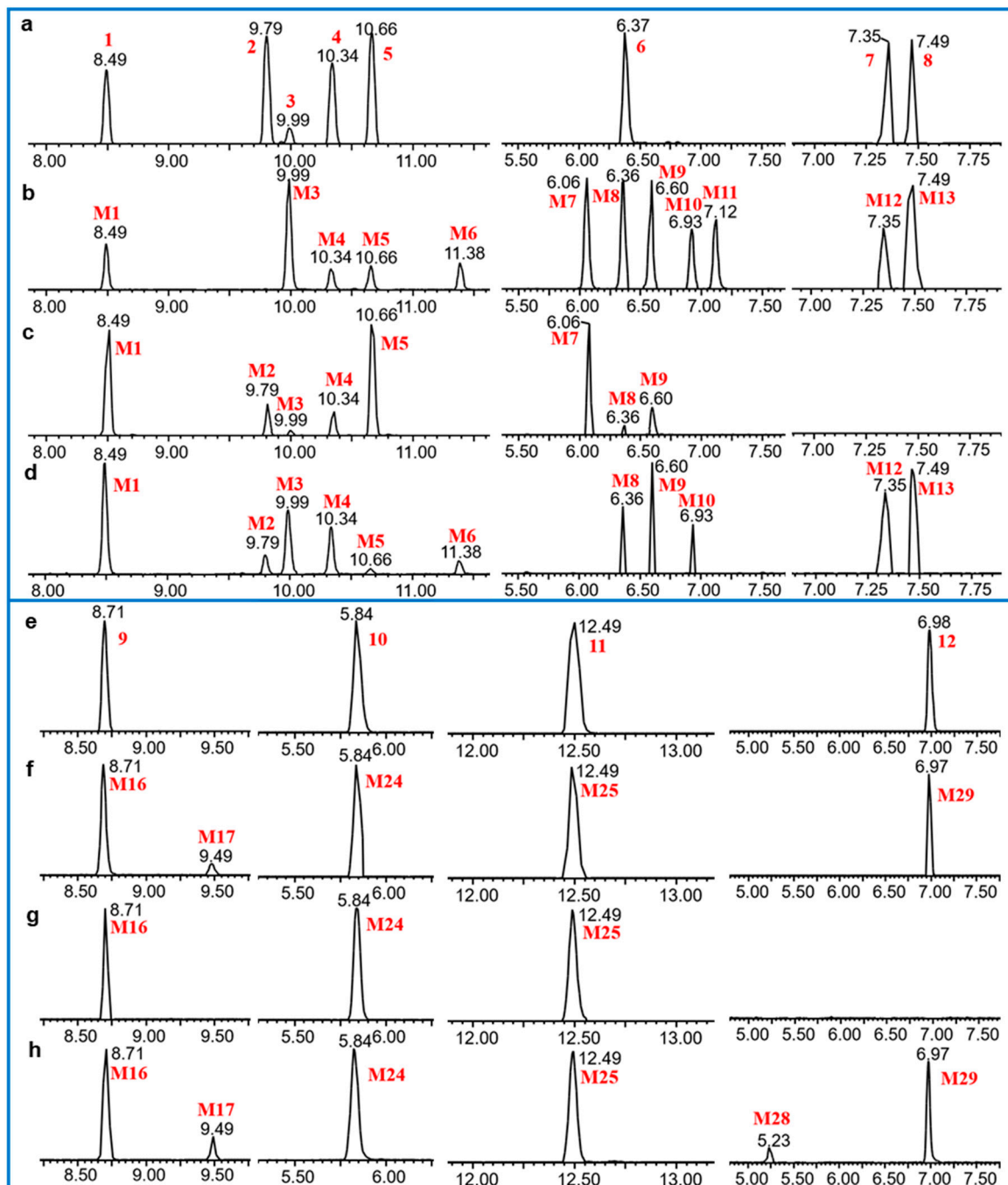


Figure 8. Extracted ion chromatograms of reference standard isolated from microbial transformation samples (a,e) and euphorbiasteroid metabolites in rat plasma (b,f), urine (c,g) and feces (d,h).

3.5. Proposed Metabolic Pathways of Euphorbiasteroid In Vivo

Based on the metabolites identified in rats (plasma, urine, and feces), RLMs and fungus mycelium (Table 4), metabolic pathways of euphorbiasteroid can be proposed.

According to the above discoveries in the metabolism of euphorbiasteroid, the hydroxylation of euphorbiasteroid was the major metabolic pathway (Figure 9), including mono-hydroxylated euphorbiasteroid (M1–M6) and dihydroxylated euphorbiasteroid (M7–M11), which undergo further metabolism to form dihydrodiol (M12–M13).

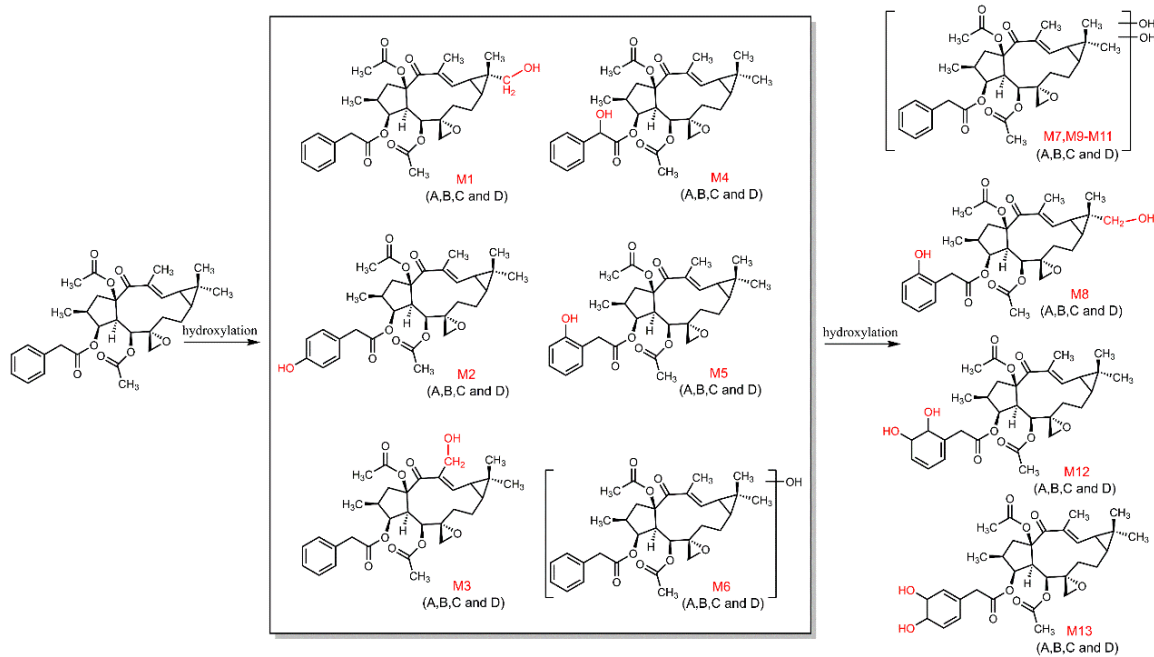


Figure 9. The proposed metabolic pathway of euphorbiasteroid in rats (I).

The second pathway involves the methyl oxidation of euphorbiasteroid, from methyl to primary alcohol, then to aldehyde group (M14–M15), and finally to carboxyl group (M16–M17) (Figure 10). In addition, the metabolites (M16–M17) were further hydroxylated to form monohydroxylated products (M18–M20) and dihydroxylated products (M21–M23).

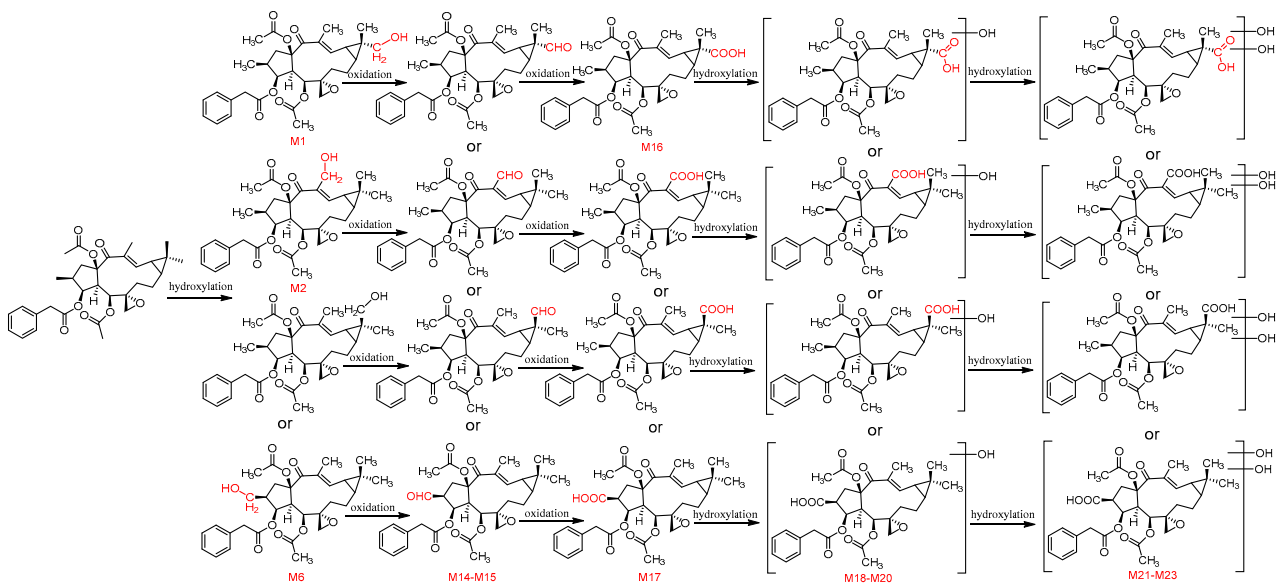


Figure 10. The proposed metabolic pathway of euphorbiasteroid in rats (II).

The third pathway involves hydrolysis of ester groups to form epoxyathyrol (**M24**) and 15-deacetyl euphorbiasteroid (**M25**), followed by hydroxylation to produce metabolites **M26–M27**, as shown in Figure 11.

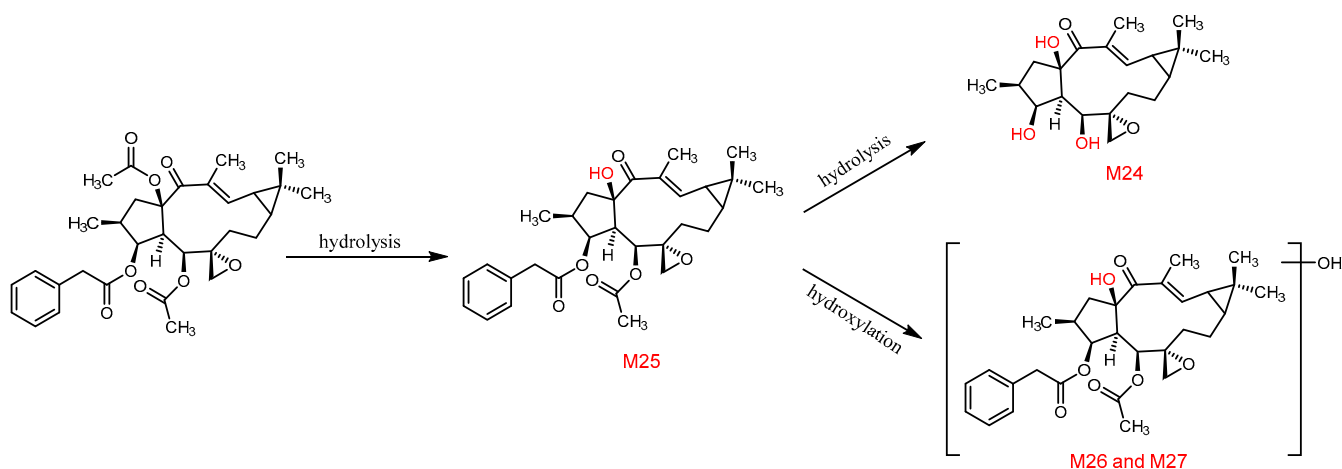


Figure 11. The proposed metabolic pathway of euphorbiasteroid in rats (III).

Finally, phase II metabolism was the predominant pathway in rat feces samples, where several metabolites were formed by glycosylation and sulfonation (Figure 12). Overall, hydroxylation, oxidation, hydrolysis, sulfonation, and glycosylation are the main metabolic pathways of euphorbiasteroid in rats.

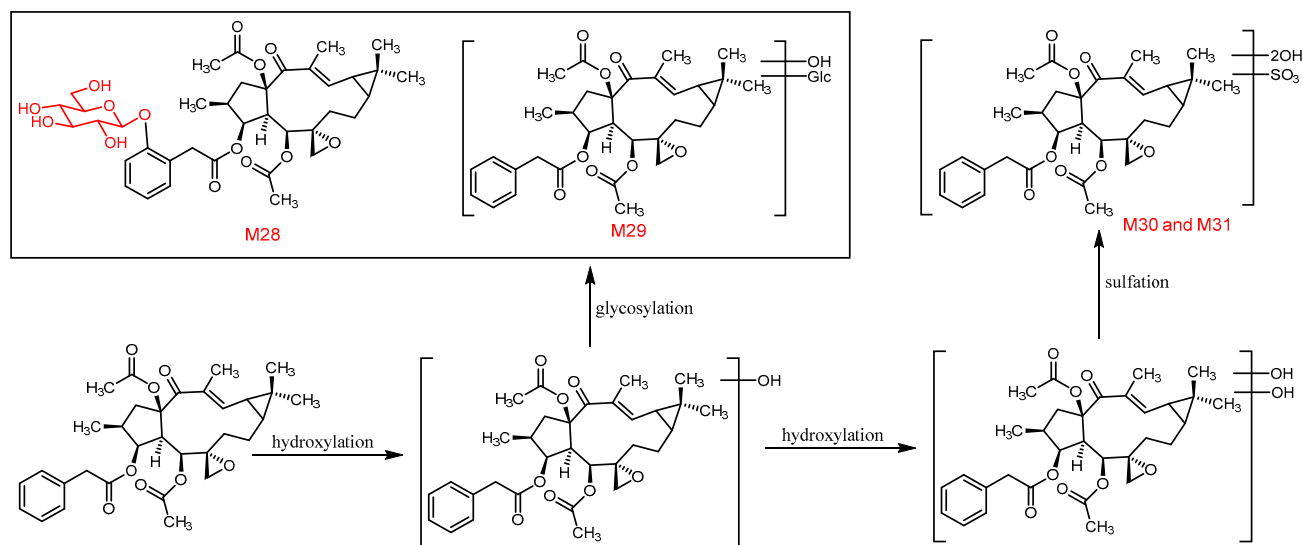


Figure 12. The proposed metabolic pathway of euphorbiasteroid in rats (IV).

3.6. Cytotoxicity of Euphorbiasteroid and Its Metabolites

Euphorbiasteroid and its metabolites were tested for their cytotoxicity on human cell lines SH-SY5Y, LO2, AC-16, and HK-2 by the CCK-8 assay. The results (Table 5) indicated that euphorbiasteroid showed no cytotoxicity against four human cell lines with IC_{50} values of more than 50 μ M. Among metabolites, the C-20 hydroxylated product **M3** (20-hydroxyl euphorbiasteroid) and two hydrolysis products **M24** (epoxyathyrol) and **M25** (15-deacetyl euphorbiasteroid) showed significant cytotoxicity against four human cell lines with IC_{50} values from 3.60 μ M to 40.74 μ M. Therefore, considering the high content of euphorbiasteroid in *Euphorbiae semen*, it was speculated that the metabolites from hydroxylation and hydrolysis might be the potential toxic constituents of *Euphorbiae semen*.

Table 5. The cytotoxicities of euphorbiasteroid and its metabolites on four strains of human cells.

Compound	IC ₅₀ (μM)			
	SH-SY5Y	LO2	AC-16	HK-2
M0	54.95 ± 1.20	>100	97.72 ± 2.13	>100
M3	39.63 ± 0.43	37.41 ± 0.41	17.86 ± 0.19	22.65 ± 0.25
M24	40.74 ± 0.44	38.9 ± 0.42	21.73 ± 0.24	26.49 ± 0.29
M25	33.27 ± 0.36	30.13 ± 0.33	3.60 ± 0.04	16.11 ± 0.18

4. Conclusions

In the present study, euphorbiasteroid metabolites generated in vivo (rat plasma, urine and feces) and in vitro (RLMs and *C. elegans* bio-110930 model) were characterized through UPLC-Q/TOF-MS. According to the molecular ions and the MS/MS fragments, a total of 31 metabolites were identified, including 27 phase I and 4 phase II metabolites. Additionally, the structures of twelve metabolites were exactly confirmed by comparing their HPLC retention times and MS/MS fragments with those of the prepared reference standards, whose structures were exactly determined based on 1D and 2D NMR analysis. The twelve identified metabolites were 18 α -hydroxyl euphorbiasteroid (**M1**), 4'-hydroxyl euphorbiasteroid (**M2**), 20-hydroxyl euphorbiasteroid (**M3**), 7'-hydroxyl euphorbiasteroid (**M4**), 2'-hydroxyl euphorbiasteroid (**M5**), 18 α ,2'-dihydroxyl euphorbiasteroid (**M8**), 5',6'-dihydroxyl dihydroeuphorbiasteroid (**M12**), 3',4'-dihydroxyl dihydroeuphorbiasteroid (**M13**), 18-carboxyl euphorbiasteroid (**M16**), epoxythyrol (**M24**), 15-deacetyl euphorbiasteroid (**M25**), and euphorbiasteroid 2'-*O*- β -D-glucopyranoside (**M29**). These results showed that the majority of phase I metabolites were generated by hydroxylation and hydrolysis, followed by oxidation and hydroxylation. Glycosylation and sulfonation played significant roles in the formation of phase II metabolites. Moreover, RLMs and *C. elegans* bio-110930 could be suitable models to simulate and prepare phase I metabolites of euphorbiasteroid. Thus, an overall description of metabolites of euphorbiasteroid from rats, RLMs and *C. elegans* bio-110930 has been provided. Three metabolites **M3**, **M24**, and **M25** exhibited potent cytotoxicity against four human cell lines. Furthermore, our study provides valuable information for predicting in vivo human metabolites and important clues for further clarifying the mechanism of drug toxicity of euphorbiasteroid and its metabolites. The method can also be applied to the study of other herbal components, providing new ideas in the field of metabolic studies of traditional Chinese medicine.

Supplementary Materials: The following supporting information can be downloaded at: <https://www.mdpi.com/article/10.3390/metabo12090830/s1>. Figure S1. HR-ESI-MS spectrum of compound **1**; Figure S2. OR Valve of compound **1** in MeOH; Figure S3. UV spectrum of compound **1** in MeOH; Figure S4. CD spectrum of compound **1** in MeOH; Figure S5. ¹H NMR spectrum of compound **1** in CDCl₃; Figure S6. ¹³C NMR and DEPT spectrum of compound **1** in CDCl₃; Figure S7. ¹H-¹H COSY spectrum of compound **1** in CDCl₃; Figure S8. HMBC spectrum of compound **1** in CDCl₃; Figure S9. HSQC spectrum of compound **1** in CDCl₃; Figure S10. NOESY spectrum of compound **1** in CDCl₃; Figure S11. HR-ESI-MS spectrum of compound **2**; Figure S12. OR Valve of compound **2** in MeOH; Figure S13. UV spectrum of compound **2** in MeOH; Figure S14. CD spectrum of compound **2** in MeOH; Figure S15. ¹H NMR spectrum of compound **2** in CDCl₃; Figure S16. ¹³C NMR and DEPT spectrum of compound **2** in CDCl₃; Figure S17. ¹H-¹H COSY spectrum of compound **2** in CDCl₃; Figure S18. HMBC spectrum of compound **2** in CDCl₃; Figure S19. HSQC spectrum of compound **2** in CDCl₃; Figure S20. NOESY spectrum of compound **2** in CDCl₃; Figure S21. HR-ESI-MS spectrum of compound **3**; Figure S22. OR valve of compound **3** in MeOH; Figure S23. UV spectrum of compound **3** in MeOH; Figure S24. CD spectrum of compound **3** in MeOH; Figure S25. ¹H NMR spectrum of compound **3** in CDCl₃; Figure S26. ¹³C NMR and DEPT spectrum of compound **3** in CDCl₃; Figure S27. ¹H-¹H COSY spectrum of compound **3** in CDCl₃; Figure S28. HMBC spectrum of compound **3** in CDCl₃; Figure S29. HSQC spectrum of compound **3** in CDCl₃; Figure S30. NOESY spectrum of compound **3** in CDCl₃; Figure S31. HR-ESI-MS spectrum of compound **4**; Figure S32. OR valve of compound **4** in MeOH; Figure S33. UV spectrum of

compound **4** in MeOH; Figure S34. CD spectrum of compound **4** in MeOH; Figure S35. ^1H NMR spectrum of compound **4** in CDCl_3 ; Figure S36. ^{13}C NMR and DEPT spectrum of compound **4** in CDCl_3 ; Figure S37. ^1H - ^1H COSY spectrum of compound **4** in CDCl_3 ; Figure S38. HMBC spectrum of compound **4** in CDCl_3 ; Figure S39. HSQC spectrum of compound **4** in CDCl_3 ; Figure S40. NOESY spectrum of compound **4** in CDCl_3 ; Figure S41. HR-ESI-MS spectrum of compound **5**; Figure S42. OR valve of compound **5** in MeOH; Figure S43. UV spectrum of compound **5** in MeOH; Figure S44. CD spectrum of compound **5** in MeOH; Figure S45. ^1H NMR spectrum of compound **5** in CDCl_3 ; Figure S46. ^{13}C NMR and DEPT spectrum of compound **5** in CDCl_3 ; Figure S47. ^1H - ^1H COSY spectrum of compound **5** in CDCl_3 ; Figure S48. HMBC spectrum of compound **5** in CDCl_3 ; Figure S49. HSQC spectrum of compound **5** in CDCl_3 ; Figure S50. NOESY spectrum of compound **5** in CDCl_3 ; Figure S51. HR-ESI-MS spectrum of compound **6**; Figure S52. OR valve of compound **6** in MeOH; Figure S53. UV spectrum of compound **6** in MeOH; Figure S54. CD spectrum of compound **6** in MeOH; Figure S55. ^1H NMR spectrum of compound **6** in $\text{C}_3\text{D}_6\text{O}$; Figure S56. ^{13}C NMR and DEPT spectrum of compound **6** in $\text{C}_3\text{D}_6\text{O}$; Figure S57. ^1H - ^1H COSY spectrum of compound **6** in $\text{C}_3\text{D}_6\text{O}$; Figure S58. HMBC spectrum of compound **6** in $\text{C}_3\text{D}_6\text{O}$; Figure S59. HSQC spectrum of compound **6** in $\text{C}_3\text{D}_6\text{O}$; Figure S60. NOESY spectrum of compound **6** in $\text{C}_3\text{D}_6\text{O}$; Figure S61. HR-ESI-MS spectrum of compound **7**; Figure S62. OR valve of compound **7** in MeOH; Figure S63. UV spectrum of compound **7** in MeOH; Figure S64. CD spectrum of compound **7** in MeOH; Figure S65. ^1H NMR spectrum of compound **7** in CDCl_3 ; Figure S66. ^{13}C NMR and DEPT spectrum of compound **7** in CDCl_3 ; Figure S67. ^1H - ^1H COSY spectrum of compound **7** in CDCl_3 ; Figure S68. HMBC spectrum of compound **7** in CDCl_3 ; Figure S69. HSQC spectrum of compound **7** in CDCl_3 ; Figure S70. NOESY spectrum of compound **7** in CDCl_3 ; Figure S71. HR-ESI-MS spectrum of compound **8**; Figure S72. OR Valve of compound **8** in MeOH; Figure S73. UV spectrum of compound **8** in MeOH; Figure S74. CD spectrum of compound **8** in MeOH; Figure S75. ^1H NMR spectrum of compound **8** in CDCl_3 ; Figure S76. ^{13}C NMR and DEPT spectrum of compound **8** in CDCl_3 ; Figure S77. ^1H - ^1H COSY spectrum of compound **8** in CDCl_3 ; Figure S78. HMBC spectrum of compound **8** in CDCl_3 ; Figure S79. HSQC spectrum of compound **8** in CDCl_3 ; Figure S80. NOESY spectrum of compound **8** in CDCl_3 ; Figure S81. HR-ESI-MS spectrum of compound **9**; Figure S82. OR Valve of compound **9** in MeOH; Figure S83. UV spectrum of compound **9** in MeOH; Figure S84. CD spectrum of compound **9** in MeOH; Figure S85. ^1H NMR spectrum of compound **9** in CDCl_3 ; Figure S86. ^{13}C NMR and DEPT spectrum of compound **9** in CDCl_3 ; Figure S87. ^1H - ^1H COSY spectrum of compound **9** in CDCl_3 ; Figure S88. HMBC spectrum of compound **9** in CDCl_3 ; Figure S89. HSQC spectrum of compound **9** in CDCl_3 ; Figure S90. NOESY spectrum of compound **9** in CDCl_3 ; Figure S91. HR-ESI-MS spectrum of compound **10**; Figure S92. ^1H NMR spectrum of compound **10** in CDCl_3 ; Figure S93. ^{13}C NMR and DEPT spectrum of compound **10** in CDCl_3 ; Figure S94. HR-ESI-MS spectrum of compound **11**; Figure S95. OR valve of compound **11** in MeOH; Figure S96. UV spectrum of compound **11** in MeOH; Figure S97. CD spectrum of compound **11** in MeOH; Figure S98. ^1H NMR spectrum of compound **11** in CDCl_3 ; Figure S99. ^{13}C NMR and DEPT spectrum of compound **11** in CDCl_3 ; Figure S100. ^1H - ^1H COSY spectrum of compound **11** in CDCl_3 ; Figure S101. HMBC spectrum of compound **11** in CDCl_3 ; Figure S102. HSQC spectrum of compound **11** in CDCl_3 ; Figure S103. NOESY spectrum of compound **11** in CDCl_3 ; Figure S104. HR-ESI-MS spectrum of compound **12**; Figure S105. OR valve of compound **12** in MeOH; Figure S106. UV spectrum of compound **12** in MeOH; Figure S107. CD spectrum of compound **12** in MeOH; Figure S108. ^1H NMR spectrum of compound **12** in CDCl_3 ; Figure S109. ^{13}C NMR and DEPT spectrum of compound **12** in CDCl_3 ; Figure S110. ^1H - ^1H COSY spectrum of compound **12** in CDCl_3 ; Figure S111. HMBC spectrum of compound **12** in CDCl_3 ; Figure S112. HSQC spectrum of compound **12** in CDCl_3 ; Figure S113. NOESY spectrum of compound **12** in CDCl_3 ; Table S1: Effects of metabolites on proliferation of four strains of human cells (Inhibition rate %).

Author Contributions: X.Z. and Y.S. designed the study, aided in funding acquisition and reviewed the manuscript. S.X., X.X. and X.W. conducted the study and analyzed the data. S.X. and X.W. drafted the original manuscript. S.L., Y.L., W.C. and B.X. aided in animal experiments. J.X. and W.Y. aided in the design of the illustrations. All authors have read and agreed to the published version of the manuscript.

Funding: The work was supported by the National Natural Science Foundation of China (82173704, 31870327, 82004215, 82073981), the Key Research and Development Program of China (2017YFC1702002, 2019YFC1711006), the National Major Project of China (2018ZX09731016-005), Shanghai Engineering

Research Center for the Preparation of Bioactive Natural Products (16DZ2280200), Shanghai Municipal Health Commission Project (20204Y0326), Three-year Action Plan for Shanghai TCM Development and Inheritance Program [ZY(2021-2023)-0401] and Sailing Program of Naval Medical University.

Institutional Review Board Statement: This study was approved by the Animal Care and Use Committee of Naval Medical University (SMMU, License No. 2019061). All animal procedures were performed in accordance with the Guideline for the Care and Use of Laboratory Animals in China.

Informed Consent Statement: Not applicable.

Data Availability Statement: The data presented in this study are available in Supplementary Materials.

Conflicts of Interest: The authors declare no conflict of interest.

Abbreviations

C. elegans, *Cunninghamella elegans*; HPLC-MS, high performance liquid chromatography-mass spectrometry; LC, liquid chromatography; NMR, Nuclear magnetic resonance; RLMs, rat liver microsomes; UPLC-Q/TOF-MS, ultra-performance liquid chromatography coupled with quadrupole time-of-flight mass spectrometry.

References

1. An, Z.; Tao, Z.; Qi, W. The phytochemistry, pharmacokinetics, pharmacology and toxicity of *Euphorbia* semen. *J. Ethnopharmacol.* **2018**, *227*, 41–55.
2. Jaretsky, R.; Köhler, W. *Euphorbia lathyris* L. als Heilpflanze. Pharmakologische Prüfungen, insonderheit des fetten Samenöls. *Arch. Pharm.* **1943**, *281*, 265–269. [[CrossRef](#)]
3. Choi, J.S.; Kang, N.S.; Yong, K.M.; Kim, S.H. Euphorbiasteroid reverses P-glycoprotein-mediated multi-drug resistance in human sarcoma cell line MES-SA/Dx5. *Phytother. Res.* **2010**, *24*, 1042–1046. [[CrossRef](#)] [[PubMed](#)]
4. Park, S.J.; Park, J.H.; Han, A.; Davaatseren, M.; Kwon, D.Y. Euphorbiasteroid, a component of *Euphorbia lathyris* L., inhibits adipogenesis of 3T3-L1 cells via activation of AMP-activated protein kinase. *Cell Biochem. Funct.* **2015**, *33*, 220–225. [[CrossRef](#)] [[PubMed](#)]
5. Wang, J.W.; Guo, F.; Zhang, C.; Ren, X.; Jiang, G.S. Mechanism of euphorbiasteroid inducing apoptosis of HL-60 cells. *China J. Cancer Prev. Treat.* **2014**, *21*, 1865–1870.
6. De Sousa, I.P.; Sousa Teixeira, M.V.; Jacometti Cardoso Furtado, N.A. An Overview of Biotransformation and Toxicity of Diterpenes. *Molecules* **2018**, *23*, 1387. [[CrossRef](#)]
7. Blanz, J.; Délémonté, T.; Pearson, D.; Luneau, A.; Ritzau, M.; Gertsch, W.; Ramstein, P.; Dayer, J.; Desrayaud, S.; Braun, E. Micropreparative isolation and NMR structure elucidation of metabolites of the drug candidate 1-isopropyl-4-(4-isopropylphenyl)-6-(prop-2-yn-1-yloxy) quinazolin-2(1H)-one from rat bile and urine. *J. Chromatogr. B Anal. Technol. Biomed. Life Sci.* **2015**, *989*, 1–10. [[CrossRef](#)]
8. Beccaria, M.; Cabooter, D. Current developments in LC-MS for pharmaceutical analysis. *Analyst* **2020**, *145*, 1129–1157. [[CrossRef](#)]
9. Xie, C.; Zhong, D.; Yu, K.; Chen, X. Recent advances in metabolite identification and quantitative bioanalysis by LC-Q-TOF MS. *Bioanalysis* **2012**, *4*, 937–959. [[CrossRef](#)]
10. Xu, L.; Liu, Y.; Wu, H.; Zhou, A. Rapid identification of absorbed components and metabolites of Gandou decoction in rat plasma and liver by UPLC-Q-TOF-MSE. *J. Chromatogr. B Anal. Technol. Biomed. Life Sci.* **2019**, *1137*, 121934. [[CrossRef](#)]
11. Li, K.; Qin, F.; Jing, L.; Li, F.; Guo, X. In vivo and In vitro metabolism of a novel beta2-adrenoceptor agonist, trantinterol: Metabolites isolation and identification by LC-MS/MS and NMR. *Anal. Bioanal. Chem.* **2013**, *405*, 2619–2634. [[CrossRef](#)]
12. Gao, Q.; Wang, D.; Shao, S.; Xue, Y.; Zhang, Y.; Chen, C.; Tang, F.; Sun, J.; Li, Y.; Guo, Q. Identification and quantitation of the actual active components in bamboo juice and its oral liquid by NMR and UPLC-Q-TOF-MS. *Sci. Rep.* **2020**, *10*, 19664. [[CrossRef](#)] [[PubMed](#)]
13. Wang, M.; Zhang, M.; Yang, Q.; Wang, Q.; Ma, B.; Li, Z.; Cheng, W.; Tang, H.; Feng, S.; Wang, Z. Metabolomic profiling of *M. speciosa* champ at different growth stages. *Food Chem.* **2021**, *376*, 131941. [[CrossRef](#)]
14. Wang, Y.D.; Song, C.G.; Yang, J.; Zhou, T.; Zhao, Y.Y.; Qin, J.C.; Guo, L.P.; Ding, G. Accurate Identification of Degraded Products of Aflatoxin B1 Under UV Irradiation Based on UPLC-Q-TOF-MS/MS and NMR Analysis. *Food Chem.* **2021**, *9*, 789249. [[CrossRef](#)] [[PubMed](#)]
15. Duan, M.; Li, Q.; Zhong, D.; Peng, Z. Identification of novel ondansetron metabolites using LC/MS n and NMR. *J. Chromatogr. B* **2018**, *1095*, 138–141. [[CrossRef](#)] [[PubMed](#)]
16. He, R.; Fan, J.; Chen, R.; Guo, D.; Zhao, M.; Zhang, Z.; Liang, C.; Chen, M.; Song, H.; Zhang, W. Stereoselective in vitro metabolism of cyproconazole in rat liver microsomes and identification of major metabolites. *Chemosphere* **2021**, *264*, 128495. [[CrossRef](#)]

17. Gaunitz, F.; Dahm, P.; Mogler, L.; Thomas, A.; Thevis, M.; Mercer-Chalmers-Bender, K. In vitro metabolic profiling of synthetic cannabinoids by pooled human liver microsomes, cytochrome P450 isoenzymes, and *Cunninghamella elegans* and their detection in urine samples. *Anal. Bioanal. Chem.* **2019**, *411*, 3561–3579. [[CrossRef](#)]
18. Nguyen, T.; Yeom, S.-J.; Yun, C.-H. Production of a Human Metabolite of Atorvastatin by Bacterial CYP102A1 Peroxygenase. *Appl. Sci.* **2021**, *11*, 603. [[CrossRef](#)]
19. Lapham, K.; Callegari, E.; Cianfrogna, J.; Lin, J.; Niosi, M.; Orozco, C.C.; Sharma, R.; Goosen, T.C. In Vitro Characterization of Ertugliflozin Metabolism by UDP-Glucuronosyltransferase and Cytochrome P450 Enzymes. *Drug Metab. Dispos.* **2020**, *48*, 1350–1363. [[CrossRef](#)]
20. Ma, Y.; Sun, P.; Zhao, Y.; Wang, K.; Chang, X.; Bai, Y.; Zhang, D.; Yang, L. A microbial transformation model for simulating mammal metabolism of Artemisinin. *Molecules* **2019**, *24*, 315. [[CrossRef](#)]
21. Yildirim, K.; Kuru, A.; Küçükbaşol, E. Microbial transformation of androstenedione by *Cladosporium sphaerospermum* and *Ulocladium chartarum*. *Biocatal. Biotransform.* **2019**, *38*, 7–14. [[CrossRef](#)]
22. Aziz, A.; Bano, S.; Atia Tul, W.; Choudhary, M.I. Microbial transformation of oral contraceptive ethisterone by *Aspergillus niger* and *Cunninghamella blakesleeana*. *Steroids* **2020**, *154*, 108467. [[CrossRef](#)] [[PubMed](#)]
23. Sponchiado, R.; Sorrentino, J.M.; Olegario, N.; Oliveira, S.S.; Cordenonsi, L.M.; Silveira, G.P.; Fuentefria, A.M.; Mendez, A.S.L.; Steppe, M.; Garcia, C.V. Microbial transformation of ambrisentan to its glycosides by *Cunninghamella elegans*. *Biomed. Chromatogr.* **2019**, *33*, e4496. [[CrossRef](#)] [[PubMed](#)]
24. Chen, C.; Song, K.; Zhang, Y.; Chu, C.; Fan, B.; Song, Y.; Huang, H.; Chen, G. Biotransformation of betulinic acid by *Circinella muscae* and *Cunninghamella echinulata* to discover anti-inflammatory derivatives. *Phytochemistry* **2021**, *182*, 112608. [[CrossRef](#)]
25. Palmer-Brown, W.; Miranda-CasoLuengo, R.; Wolfe, K.H.; Byrne, K.P.; Murphy, C.D. The CYPome of the model xenobiotic-biotransforming fungus *Cunninghamella elegans*. *Sci. Rep.* **2019**, *9*, 9240–9248. [[CrossRef](#)]
26. Asha, S.; Vidyavathi, M. *Cunninghamella*—A microbial model for drug metabolism studies—A review. *Biotechnol. Adv.* **2009**, *27*, 16–29. [[CrossRef](#)] [[PubMed](#)]
27. Xiao, S.J.; Li, S.S.; Xie, B.; Chen, W.; Xu, X.K.; Zu, X.P.; Shen, Y.H. Systematic characterization of metabolic profiles of ingenol in rats by UPLC-Q/TOF-MS and NMR in combination with microbial biotransformation. *RSC Adv.* **2021**, *11*, 37752–37759. [[CrossRef](#)]
28. Wintermeyer, A.; Möller, I.; Thevis, M.; Jübner, M.; Beike, J.; Rothschild, M.A.; Bender, K. In vitro phase I metabolism of the synthetic cannabimimetic JWH-018. *Anal. Bioanal. Chem.* **2010**, *398*, 2141–2153. [[CrossRef](#)]
29. Baydoun, E.; Atia-tul-Wahab; Mehmood, H.; Ahmad, M.S.; Malik, R.; Smith, C.; Choudhary, M.I. Microbial transformation of danazol with *Cunninghamella blakesleeana* and anti-cancer activity of danazol and its transformed products. *Steroids* **2016**, *105*, 121–127. [[CrossRef](#)]
30. Wang, Y.; Xiang, L.; Wang, Z.; Li, J.; Xu, J.; He, X. New anti-neuroinflammatory steroids against LPS induced NO production in BV2 microglia cells by microbial transformation of isorhodeasapogenin. *Bioorg. Chem.* **2020**, *101*, 103870. [[CrossRef](#)]
31. Sun, J.H.; Yang, M.; Wang, X.M.; Xu, M.; Liu, A.H.; Guo, D.A. Identification of tanshinones and their metabolites in rat bile after oral administration of TTE-50, a standardized extract of *Salvia miltiorrhiza* by HPLC-ESI-DAD-MSn. *J. Pharm. Biomed. Anal.* **2007**, *44*, 564–574. [[CrossRef](#)] [[PubMed](#)]
32. Zhang, J.; Jiang, M.; Yue, Z.; Wang, Z.; Wang, H.; Chen, M.; Wei, X.; Shi, S.; Wang, M.; Wang, Y. Characterization of diterpene metabolism in rats with ingestion of seed products from *Euphorbia lathyris* L. (*Semen Euphorbiae* and *Semen Euphorbiae Pulveratum*) using UHPLC-Q-Exactive MS. *Biomed. Chromatogr.* **2022**, *36*, e5394. [[CrossRef](#)] [[PubMed](#)]
33. Šuláková, A.; Nykodemová, J.; Palivec, P.; Jurok, R.; Rimpelová, S.; Leonhardt, T.; Šichová, K.; Páleníček, T.; Kuchař, M. 25CN-NBOMe Metabolites in Rat Urine, Human Liver Microsomes and *C.elegans*-Structure Determination and Synthesis of the Most Abundant Metabolites. *Metabolites* **2021**, *11*, 212. [[CrossRef](#)]
34. Nykodemová, J.; Šuláková, A.; Palivec, P.; Češková, H.; Rimpelová, S.; Šichová, K.; Leonhardt, T.; Jurásek, B.; Hájková, K.; Páleníček, T.; et al. 2C-B-Fly-NBOMe Metabolites in Rat Urine, Human Liver Microsomes and *C. elegans*: Confirmation with Synthesized Analytical Standards. *Metabolites* **2021**, *11*, 775. [[CrossRef](#)] [[PubMed](#)]
35. Grafinger, K.E.; Stahl, K.; Wilke, A.; König, S.; Weinmann, W. In vitro phase I metabolism of three phenethylamines 25D-NBOMe, 25E-NBOMe and 25N-NBOMe using microsomal and microbial models. *Drug Test. Anal.* **2018**, *10*, 1607–1626. [[CrossRef](#)]
36. Bicchì, C.; Appendino, G.; Cordero, C.; Rubiolo, P.; Ortellì, D.; Veuthey, J.L. HPLC-UV and HPLC-positive-ESI-MS analysis of the diterpenoid fraction from caper spurge (*Euphorbia lathyris*) seed oil. *Phytochem. Anal.* **2001**, *12*, 255–262. [[CrossRef](#)]